SACLANTCEN Conference Proceedings No. 17 Part 2

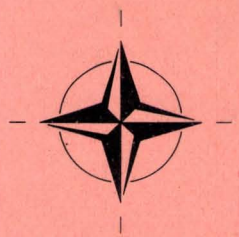

SACLANTCEN
Conference Proceedings No. 17

PART 2
BUBBLES

SACLANT ASW
RESEARCH CENTRE

OCEANIC ACOUSTIC MODELLING

Proceedings of a Conference held at SACLANTCEN on 8-11 September 1975

Organized by

WOLFGANG BACHMANN and ROBERT BRUCE WILLIAMS

15 OCTOBER 1975

NORTH
ATLANTIC
TREATY
ORGANIZATION

VIALE SAN BARTOLOMEO 400
I - 19026 - LA SPEZIA, ITALY

Compiled and Published by

STI

SACLANTCEN

SACLANTCEN
CONFERENCE PROCEEDINGS NO. 17

NORTH ATLANTIC TREATY ORGANIZATION
SACLANT ASW Research Centre
Viale San Bartolomeo 400
I 19026 - La Spezia, Italy

OCEANIC ACOUSTIC MODELLING

Proceedings of a Conference held at SACLANTCEN
on 8-11 September 1975

In eight parts

Part 2: Bubbles

Organized by
Wolfgang Bachmann and Robert Bruce Williams

15 October 1975

PAPERS PRESENTED AT CONFERENCE

Pt 1: Noise (and Introductory Matter)

1. A.W. Pryce, "Keynote address: Underwater acoustics — modelling".
2. P. Wille, "Noise sources in the ocean, Pt I".
3. M. Daintith, "Noise sources in the ocean, Pt II".
4. H. Cox, "Acoustic noise models".

Pt 2: Bubbles

5. B. Williams & L. Foster, "Gas bubbles in the sea: A review and model proposals".
6. H. Medwin, "Acoustical probing for microbubbles at sea".

Pt 3: Sea surface

7. C.R. Ward, "A spectral ocean wave model".
8. H. Schwarze, "A theoretical model for doppler spread of backscattered sound from a composite-roughness sea surface".
9. O.I. Diachok, "Effects of sea-ice ridges on sound propagation in the Arctic Ocean".
10. J. Siebert, "Low-frequency acoustic measurements in a shallow-water area with a rough sea surface".
11. P.A. Crowther, "Surface wave spectra".
12. H. Trinkaus, "Scattering and reflection of sound from the sea surface".

Pt 4: Sea bottom

13. F.M. Phelan, B. Williams & F.H. Fisher, "Highlights of bottom topography inferred from received depression and bearing angles".
14. S.R. Santaniello & F.R. Dinapoli, "Ocean-bottom reflectivity (a point of view)".
15. W.A. Kuperman & F. Ingenito, "Relative contribution of surface roughness and bottom attenuation to propagation loss in shallow water".
16. R.E. Christiensen & W.H. Geddes, "Refraction of sound in the sea floor".
17. J.A. Desanto, "Scattering from a random interface".
18. E.L. Hamilton, "Acoustic properties of the sea floor".
19. H. Bucker & H. Morris, "Reflection of sound from a layered ocean bottom".
20. B. Hurdle, K.D. Flowers & J.A. Desanto, "Acoustic scattering from rough surfaces".

Pt 5: Macro-scale phenomena

21. W. Munk, "Acoustic scintillations of acoustic waves".
22. S. Flatté, "Intensity and phase fluctuations in low-frequency acoustic transmission through internal waves".
23. T.H. Bell, Jr., J.M. Bergin, J.P. Dougan, Z.C.B. Hamilton, W.D. Morris, B.S. Okawa, E.E. Rudd & J. Witting, "Two-dimensional internal-wave spectra".
24. I.M. Blatstein, "Ocean-basin reverberation from large underwater explosions, Pt I: Source-level and propagation-loss modelling".
25. J.A. Goertner, "Ocean-basin reverberation from large underwater explosions, Pt II: Computer model for reverberation".
26. J.D. Shaffer, R.M. Fitzgerald & A.N. Guthrie, "Some effects of large-scale oceanography on acoustic propagation".
27. H.H. Essen, "Influence of internal waves on sound propagation in the SOFAR channel".
28. O.M. Johannessen, "A review of oceanic fronts".
29. R. Mellen & D.G. Browning, "Some acoustic effects of internal macrostructure".

Pt 6: Micro-scale phenomena

30. D.R. Del Balzo & W.B. Moseley, "Random temperature structure as a factor in long-range propagation".
31. J.J. McCoy, "Beam spreading and loss of spatial coherence in an inhomogeneous and fluctuating ocean".
32. R. Tait, "Internal oceanographic microstructure phenomena".
33. D. Mintzer, "Acoustic effects of internal microstructure".

Pt 7: Field calculations

34. S.N. Wolf, "Measurements of normal-mode amplitude functions in a nearly-stratified medium".
35. R.D. Graves, A. Nagl, H. Uberall, A.J. Haug & G.L. Zarur, "Range-dependent normal modes in underwater sound propagation".
36. J.A. Desanto, "Inverse wave propagation in an inhomogeneous waveguide".
37. A. Gille & D. Odero, "A solution of the wave sound equation in shallow water for real-speed profiles and solid bottom under-sediment".
38. D.J. Ramsdale, "A wave-theoretic method for estimating the effects of internal tides on acoustic wave transmission".
39. J.G. Schothorst, "Effect of ship motion on sonar detection performance".
40. C.W. Spofford & H. Garon, "Deterministic methods of sound-field computation".
41. R. Goodman, "Stochastic methods of sound-field computation".

Pt 8: Sonar models

42. B.B. Adams & G.R. Giellis, "A technique of comparative analysis of underwater-sound-transmission loss curves".
43. J.A. Desanto, "Connection between the solution of the Helmholtz and parabolic equations for sound propagation".
44. F. Dinapoli, "Computer models for underwater-sound propagation".
45. D. Wood, "Assessment techniques for computer models of sound propagation".

TABLE OF CONTENTS

Pt 2: Bubbles

	Pages
REVIEW PAPERS	
B. Williams and L. Foster. Gas bubbles in the sea. A review and model proposals.	5-1 to 5-23
H. Medwin. Acoustic probing for microbubbles at sea.	6-1 to 6-29
DISCUSSION	
R.F.J. Winterburn. Discussion on Session 2	D2-1

(Total number of printed pages in this document: 56)

REVIEW PAPERS

GAS BUBBLES IN THE SEA: A REVIEW AND MODEL PROPOSALS

by

Robert Bruce Williams and Leslie A. Foster
SACLANT ASW Research Centre
La Spezia, Italy

ABSTRACT

The literature pertaining to both free bubbles (Pt 1) and bubbles associated with fish anotomy (Pt 2) is reviewed with particular emphasis on their distributions in the sea and influencing factors. An attempt is made to compact the results to date into simple, mostly empirically-based models. Some of the models proposed contrast with those previously used. For example, depth dependence of free-bubble concentrations is proposed to be simply influenced by pressure, which causes a $(\text{depth})^{-2/3}$ relationship for Medwin's 1970 data (radius > 60 micrometres) for depths greater than 10 metres, while at shallower depths the dependence is less. In refitting data of fish-bladder volume to be proportional to $(\text{length})^{N}$, N was strongly dependent on the type of fish, and in all cases, N was larger than previously accepted. Finally, a free-bubble concentration-function model is proposed which is a linear sum of functions of a single generating mechanism (waves, rain, photosynthesis, etc.). Although this last step may be premature from the standpoint of our present knowledge of the subject, it supplies a basic structure and aids in clarifying where knowledge is lacking.

PART 1 FREE BUBBLES

INTRODUCTION

Knowledge of gas bubbles in the sea becomes important in many diverse subjects, which include:

Visibility in the lower atmosphere;

cloud formation due to salt particles injected into the air by bursting bubbles;

underwater acoustic-propagation characteristics such as absorption, scattering and sound-speed modification;

acoustic noise;

exchanges of properties at the air/sea interface, such as water, gases, heat, salt, and bacteria;

sea-surface chemistry, such as fractionation processes;

vertical transport of a variety of properties due to the scavenging effect of the bubbles.

Although this list is quite encompassing, relatively little work has been devoted to the study of gas bubbles in the sea and very few measurements of bubble concentration and size distributions have been made.

The first measurement of sea bubbles were those of Blanchard and Woodcock (1957), hereafter referred to as B &W, who, motivated by the problems of salt-nuclei formation in the atmosphere, made some near-beach estimates of bubble concentrations from breaking waves. Glotov et al (1962) studied bubble formation in a tank with various wind speeds. But by far the most work has come from Medwin (1970, 1974, 1975) and his associates at the Monterey U.S. Naval Post-Graduate School. His measurements range over depths of 5 to 45 ft in different sea states, different locations, and with different techniques. The purpose of this paper is to review what has been measured and what models have been put forth to date, condense this information into cohesive models that reflect the various data, and point out what information is lacking.

1. VERTICAL VELOCITY AND GAS DIFFUSION

B &W set the frictional (Stokean) drag force equal to the buoyancy force, and derived a relationship between the bubble radius, R, and the vertical velocity, w:

$$R = \frac{3}{8} \frac{C_d}{g} w^2 , \qquad \text{[Eq. 1]}$$

g being the acceleration due to gravity and C_d the spherical drag coefficient (Goldstein, 1938). They compare this with the measurements of Allen (1900) and show good agreement in the range of his measurements, $10^2\ \mu m < R < 10^3\ \mu m$.

Le Blond (1969) notes that in all but the cleanest of liquids, the vertical velocity of a gas bubble for small Reynolds numbers is given by the solid sphere formula:

$$w_d = \frac{2}{3} g \frac{R^2}{\nu} , \qquad \text{[Eq. 2]}$$

instead of the Rybezynaki-Hadamand expression for a gas sphere:

$$w_c = \frac{1}{3} g \frac{R^2}{\nu} \qquad \text{[Eq. 3]}$$

where ν is the kinetic viscosity of the liquid, and where the subscripts d and c refer to dirty and clean bubbles, respectively. The supposition is that minute particulate or organic matter forms a film around the bubble. In addition, for small Reynolds numbers, the mass flux of gas out of the bubble is given by

$$F_c = 24\left(\frac{\pi g D}{2\nu}\right)^{\frac{1}{2}} R^{\frac{1}{2}}(C - C_\infty)$$

$$F_d = 72\left(\frac{2gD^2}{9\nu}\right)^{\frac{1}{3}} R^{\frac{4}{3}}(C - C_\infty) \qquad \text{[Eq. 4]}$$

where D is the diffusivity of the gas,

C is the concentration (g/cm^3) in the bubble, and

C_∞ is the concentration far away from the bubble.

He states that Eqs. 2, 3 and 4 apply for $r < 80\ \mu m$. We note that Eq. 1 reduces to Eq. 3 with:

$$C_D = \frac{24\ \nu^2}{gR^3} .$$

Datta, et al (1950) have noted that bubbles greater than about 1 mm radius tend to zig-zag in their ascent, and that their vertical velocity may even become less than that of a slightly smaller radius. Furthermore, a plateau is reached where w remains constant for radii between 2 and 7 mm. In this region, distortions from the spherical shape are seen.

Turner (1972) has made an analysis of the deformation of large bubbles in a high Reynolds number ascent, and shows that the shape is like that of an umbrella, or a mature atomic-bomb cloud. In terms of an equivalent radius, whose volume is the same as the deformed bubble,

$$\omega = \frac{2}{3}\left(g\frac{R}{\alpha}\right)^{\frac{1}{2}}, \quad \alpha = 0.49 \pm 0.09 \ . \qquad \text{[Eq. 5]}$$

However, bubbles of this size tend to break up. Note that this is the same as Eq. 1, with $C_D = 1$.

To summarize, for small radii (< 80 μm) Eqs. 2 or 3 can be used for vertical velocity. For radii up to 1 mm, the more general equation [Eq. 1] is necessary. From 2 mm to 7 mm, it appears that the best prediction for the velocity is a constant (25 cm/s). Above a 7 mm equivalent radius, Eq. 5 must be used. Equation 4 describes the gas flux out of the bubble for small ($r < 80$ μm) bubbles. To our knowledge, there are no predictions of gas flux for larger bubbles.

2. LIFETIME OF BUBBLES

By considering only gas saturation, a bubble might be expected to lose some of its gas by diffusion and therefore its volume will be expected to diminish if the sea is undersaturated while a bubble in supersaturated water would be expected to grow. However, additional factors need to be included to predict the evolution of a bubble. B & W have extended the calculations of Wyman et al (1952) regarding the rate of growth of a bubble, taking into account the surface tension effects, which are of prime importance for small bubbles. Figure 1 shows these lifetime calculations vs bubble diameter for different saturation percentages at 10 cm depth. The result is that for a given supersaturation there exists a depth below which bubbles of any radius will go into solution. That depth is simply given by

$$d = 10\ (x-1) \text{ metres} \qquad \text{[Eq. 6]}$$

where x is the fraction of saturation. Thus, for example, all bubbles deeper than 1 metre will go in solution in 110% super-saturated waters.

Turner (1961) found that, in laboratory experiments, small bubbles can persist for long periods of time, or indefinitely in apparent contradiction to the results of B & W. However, he attributes this persistence to particulate matter in the water, possibly forming "walls" around the bubble so as to support excess pressure and block gas diffusion. Even small amounts of particulate matter in the water produced lifetimes greater than 100 hours.

Le Blond (1969) studies theoretically the problem of gas diffusion in an ascending bubble. He points out that even in subsaturated water a bubble may grow in volume provided its ascending velocity is large enough so that the ambient pressure decreases faster than the pressure reduction due to loss of gas by diffusion.

His model predicts the existences of two critical radii: r_a, above which the volume will grow; and r_b, below which the gas pressure increases while the volume shrinks and ultimately collapses. The fate of bubbles whose radii lie in between r_a and r_b cannot be easily predicted from his model, but must either ultimately grow or collapse.

For velocities in the Stoke's regime, Le Blond has explicit expressions for r_a and r_b:

$$r_a = \left[\frac{3\nu}{\alpha g}\,\beta_c (P - \gamma)\right]^{2/5}$$

$$r_b = \left(\frac{2\sigma}{3P}\right)^{2/7} r_a^{\,5/7} \qquad \text{[Eq. 7]}$$

$$\gamma = \frac{C_\infty}{K}\,, \quad \beta_c = 8\left(\frac{\pi g D}{2\nu}\right)^{\frac{1}{2}} K$$

where the coefficient of absorption (Dorsey 1940, p.529), $K = \frac{C}{P}$. C is the concentration of gas in the liquid at the gas-liquid interface, P the pressure inside the bubble and σ the surface tension. In addition, he also gives formulas for "dirty" bubbles. But, as he points out, for the dirty bubbles, the effective value of K would be reduced an unknown amount, casting doubt on its validity. In any case, the critical radii are lowered by the presence of a surface coating on the bubble, making upper bounds of the clean bubble estimates of critical radii.

3. BUBBLE GENERATION MECHANISMS

This chapter reviews briefly the research on the various bubble-generation mechanisms; details and implications of these results will be discussed in Ch. 4.

3.1 Surface-wave generation

The measurements of B & W pertain to surface waves breaking, although it is not clear whether the breaking is due to waves shoaling or due to the wind. Their measurements were made at a 10 cm depth near the beach with fresh winds on shore. There was a strong monotonic decrease in the number of bubbles as the radius increased through the range of measurements from 37 μm to 250 μm.

Glotov, et al (1972) have studied wave generation of bubbles in a 3 m deep tank at different laboratory-generated wind speeds. Both acoustic and optical determination of the bubble concentrations were made at a depth of 1.5 m. Their technique provided measurements of bubbles from 27 to 137 μm radius. They report that relatively few bubbles are formed at wind speeds of less than 10 m/s, while an abrupt increase in bubbles is observed for speeds of greater than 10 m/s, when whitecaps are formed. These wind speeds are not directly applicable to the open ocean, due to the restricted fetch in the laboratory. However, there may be some means of relating the measurements to open sea conditions.

Unfortunately, they do not report actual values of bubble concentrations, although they do describe a relative bubble concentration function vs radius. They further state that the shape of this function is almost independent of wind speeds for winds greater than 10 m/s.

As noted before, most of our present knowledge of bubbles in the sea comes from Medwin and his associates. For over a decade, they have been developing different methods of detection of bubbles and have been making ocean measurements, principally in coastal waters. Their measurements span depths from 1.5 to 15 m, radii from 18 to 180 μm and conditions from sea state one to winds of 14 m/s. Details of these works are given in Ch. 4. Their detection techniques include the use of acoustic absorption, scattering, and dispersion; optical techniques were used in earlier studies to verify the acoustic methods.

3.2 Precipitation — Rain, Snow and Dust

B & W have made laboratory measurements of bubble production of simulated rain to study the dependence of drop size on the generation of bubbles. They found that small drops (200 μm radius) will produce two or three 25 μm radius bubbles that are carried 1 to 3 mm below the surface. However, large drops (> 2000 μm radius) can produce well over 200 bubbles to depths of 2 to 4 cm. The vast majority of the bubbles are under 25 μm radius. They point out that the bubbles are formed by both the direct impact of the drop, and also by the splashed drops it creates.

B & W also found snow to be a significant factor in creating bubbles. From fifty to several hundred bubbles are produced by the melting of a single snowflake. Using a low-power microscope, they are able to produce a bubble-size distribution function. We have found that his function fits fairly well to

$$P(R) = \left(\frac{R}{b}\right) e^{-(R/a)^3}, \qquad \text{[Eq. 8]}$$

with $b = 50\ \mu m$, $a = 30\ \mu m$. $P(R)\Delta R$ is the probability of a bubble having a radius between R and $(R + \Delta R)$. During these measurements, they observed that bubbles with a radius smaller than 15 μm grew

smaller, while those greater than 25 μm grew larger, in agreement with the analysis of the Le Blond (1969). Therefore, P(R) will evolve with time, and Eq. 8 is only appropriate for times that are small compared with a bubble's lifetime.

Medwin (1970) has suggested that some of the bubbles he observed were due to either photosynthesis or continental dust carrying air into the water. The radii of these bubbles ranged from 18 μm (lower limit of observation) to 50 μm. He observes a reduction in their numbers at night. The question of origin of these bubbles is further discussed in Ch. 4.

3.3 Photosynthesis

LaFond and Dill (1952) have made measurements of various properties of a costal-water region, including oxygen content and turbidity. They take the oxygen supersaturated top layer as evidence for photosynthetic activity in the underlying turbid layer observed between 15 and 25 feet depth. However, the only direct evidence for bubbles comes from the observations of foam lines on the surface. They also point out that the origin of these bubbles could also be due to the following mechanism.

3.4 Heating of Saturated Waters

There is no direct measurements of bubbles formed by the heating of waters saturated with gas. However LaFond and Dill observed that foam was associated with coastal slicks and speculated that this might be due to this mechanism. On an annual basis, the waters give off air in the spring/summer seasons that was stored in the fall/winter months. If this gas is given off in the form of 25 μm bubbles, the flux would be 2500/cm^2/s through the surface (B & W), much longer than any bubble observations. Undoubtedly, most of the air exchange is due to molecular diffusion at the surface, but if strong heating occurs with weak or no vertical mixing, it is easily possible to form many bubbles.

3.5 Bubbles of Biological Origin

Although it is well known that bubbles are released by fish, quantitative estimates are lacking in the literature.

3.6 Bubbles due to Chemical Decomposition

McCartney and Barry (1965) report observations with an echo sounder of bubbles forming on a 200 m depth bottom. The size, inferred from the vertical velocity, was from 450 to 750 μm radius at the bottom, with a distribution of 85% between 550 to 600 μm. They further state that there were no bubbles produced at 50 and 300 μm radii. The bottom conditions were anaerobic, and therefore possibly

methane was the bubble gas. The actual volume fraction of gas in these waters due to these bubbles is about 3×10^{-15}, seven to ten orders of magnitude smaller than wave-generated bubbles near the surface.

3.7 Surface Emission by Bursting Bubbles

MacIntyre (1972) has studied some of the physics in breaking bubbles at the surface, showing that during millimetre-size bubble collapse, many small bubbles are injected back into the water. These bubbles ($< 50\,\mu m$ radius) are injected a centimetre or two below the surface, but then could be carried downward further by water motions. It is possible that the smallest bubbles measured by B & W at a 10 cm depth are due to this mechanism.

4. BUBBLE CONCENTRATIONS

4.1 Description Method

Although there are various ways of describing the bubble concentrations, we will follow the method of B & W and Medwin, using the units of Medwin. The basic function is the number of bubbles per cubic metre per micrometre (micron) increment of radius, $\psi(R)$, or "bubble spectrum". Multiplying this function by $4/3\pi R^3$ will yield the gas fraction volume per micrometre radius increment, and integrating this with respect to R from zero to infinity will yield the gas fraction volume due to all bubbles.

We write the total bubble concentration as a sum of the separate bubbles concentrations generated by the various mechanisms in the previous section.

$$\Psi = \Psi_W + \Psi_P + \Psi_{Ph} + \Psi_{SS} + \Psi_B + \Psi_C + \Psi_{SE} \qquad \text{[Eq. 9]}$$

where the subscripts W, P, Ph, SS, B, C, SE refer to the generating processes of waves, precipitation, photosynthesis, supersaturation, biological, chemical decomposition, and surface emission respectively. The individual bubble spectra are then discussed separately when possible.

4.2 Wave-inducted Bubble Concentrations, Ψ_W

Figure 2 shows the results of B & W at d = 10 cm depth, indicating that Ψ is consistent with an R^{-5} dependence up to about 300 μm radius. Although the data measured on the leeside of a rock can also be fitted to a R^{-5} function, we will not use it in

subsequent discussion. B & W state that its lower values may be due to either wind shielding by the rock, or due to a lower wind speed at the time of measurement. In either case, B & W seem to feel that their measurements of bubble concentration are dependent on the wind, rather than the shoaling and subsequent breaking of waves.

An example of Medwin's scatter derived data (1970) in Fig. 3 shows the sea-state dependence at a 10 ft depth. For bubbles smaller than 60 μm, the dependence is not evident. These bubbles are not believed to be due to waves and are left for later discussions. Figure 4 displays some of Medwin's absorption derived data, which have been multiplied by the volume of the bubble to produce the "fractional bubble volume spectrum". Bubbles smaller than 60 μm have a day/night dependence, while at the larger radii this dependence is not as striking. The R^1 dependence corresponds to an R^{-2} dependence in Ψ from 60 μm to 180 μm (upper limit of observations).

The result of tank experiments of Glotov et al (1962) are shown in Fig. 5. They state that the shape is independent of wind speed, W, for $W \geq 10$ m/s. This speed, at which the onset of whitecaps is noted, corresponds perhaps to 6 m/s in the open ocean when the same event occurs. To rationalize this shape with the measurements of Medwin and B & W requires some speculation. Although the region above 100 μm is consistent with B & W (R^{-5}), there is a lessening of slope and eventual decreasing of Ψ for smaller radii. It is possible that at the shallow depth of the measurements of B & W (10 cm) surface emission (Ψ_{SE}) also contributed to the small radii portion of Ψ. Since Medwin's 1970 data were measured at sea states 1 and 2, it is not expected that his shape would have "evolved" to that of Glotov et al. However, going from sea state 1 to 2, indicates a steepening of slope for $R > 100$ μm (Fig. 3) and may indicate that the spectrum is becoming more similar to that of Glotov as wind speeds increase.

In an attempt to assess the wind dependence of Ψ, we have tabulated some gas-volume fraction data (Table 1), mostly at 3 m depth (see Fig. 6). It appears that the differential speed method results in a different wind speed dependence than the other two methods. B & W's data may be extrapolated by the depth-dependence model described later. In addition, some of the value can be attributed to surface emission, Ψ_{SE}, but certainly no more than 50%. Finally an equivalent wind speed must be estimated, probably greater than 6 m/s but perhaps no more than 15 m/s. The resulting B & W estimate is still a factor of thirty higher than Medwin's (1975) 14 m/s value, and is more in agreement with the other values.

It is obvious that too few measurements exist to give an accurate estimate of wind-speed dependence. However, in the spirit of creating a simple model that describes the existing data, the following wind dependence is offered, which is consistent with estimating W = 12 m/s for the data of B & W with 1/3 of the volume fraction due to surface emission.

$$U(W) = AW^3 \qquad \text{[Eq. 10]}$$

where U is the volume fraction of gas, W is wind speed in m/s and $A = 3.7 \times 10^{-9} s^3/m^3$.

TABLE 1

VOLUME GAS FRACTION

Investigator	W(m/s)	u	Depth (m)
Medwin 1970 Absorption method	1	4.7×10^{-8}	3
Medwin 1970 Scattering method	1	4.0×10^{-8}	3
Medwin 1970 Scattering method	2	2.2×10^{-7}	3
Medwin 1975 Differential speed method	12-15	1.9×10^{-7}	3
B & W	?	1.7×10^{-5}	0.1
B & W Extrapolated to 3 m	?	1.1×10^{-5}	3
B & W Extrapolated to 3 m assuming 50% due to surface emission	?	5.5×10^{-6}	3

Equation 10 has the characteristics that U(0) = 0, while U(W) increases rapidly with W, as noted by Glotov. However, it may be in error both in form and value due to the crude estimates necessary for its establishment: again if the shape of Ψ is independent of W, then:

$$u \propto \Psi \propto W^3 .$$

Medwin reports a depth dependence proportional to $d^{-\frac{1}{2}}$ for iso-frequency measurements. However, the resonant frequency for $d > 10$ m has a $d^{-\frac{1}{2}}$ dependence, indicating perhaps no depth dependence of Ψ for a constant R. A simple, physically-tractable depth-dependence model would be for a well-mixed layer in which the lifetime of the bubbles,

$$\tau \gg \frac{d}{u} \quad \text{and} \qquad \text{[Eq. 11]}$$

$$u \gg w$$

where u is a characteristic water velocity, d is the depth, and w is the vertical velocity of the bubble. In this case, the radius of the bubble will have a depth dependence from the ideal gas law:

$$R(d) = \frac{R(0)}{(1+\frac{d}{10})^{\frac{1}{3}}} . \qquad \text{[Eq. 12]}$$

For example, Medwin's data would have a form

$$\Psi(R, d) = b(1 + \frac{d}{10})^{-\frac{2}{3}} R^{-2}$$

in the region of $60\,\mu m < R < 130\,\mu$. We have fitted his data to a R^{-2} dependence for each depth, calculating $\Psi(100\,\mu m)$ from the fit. The values of $\Psi(100)$ are plotted vs depth in Fig. 7, along with the prediction of Eq. 12. The fit seems reasonable for depths down to 25 ft, but for greater depths Ψ is higher than the model. If the assumptions of Eq. 11 are violated, then Ψ should be less than the prediction of a "well mixed" model, since some bubbles will be going into solution faster at the greater depths. A possible explanation is that there is a source of bubbles at depth possibly photosynthetic, increasing the population.

From the above discussions, the following model for $\Psi(R, W, d)$ is proposed:

$$\Psi_W(R,W,d) = C_1 W^3 (1+\frac{d}{10})^{-\frac{5}{3}} R^{-5} \qquad 80\,\mu m < R < 300\,\mu m$$

$$\Psi_W(r,W,d) = C_2 W^3 (1+\frac{d}{10})^{-\frac{1}{3}} R^{-1} \qquad 50\,\mu m < R < 80\,\mu m \qquad \text{[Eq. 13]}$$

which is a compromise between the spectrum shapes of B & W, Glotov, and Medwin. $C_1 = 9 \times 10^{10}$, $C_2 = 4.5 \times 10^1$, d in metres, W in m/s, R in micrometres and Ψ in bubbles per cubic metre per micrometre radius increment. For low W, the shape will not be in agreement with Medwin, and for $50\,\mu m < R < 80\,\mu m$, the slope is between B & W and Glotov, favouring Glotov, since we feel that the small bubbles close to the surface may be due to surface effects, and are accounted for in Ψ_{SE}.

4.3 Bubble Concentrations due to Photosynthesis, Ψ_{Ph}

Bubbles in the region $18\,\mu m < R < 50\,\mu m$ measured by Medwin (1970) are believed not to be due to waves but possibly to photosynthesis because they do not appear to have a sea-state dependence, and it appears that their source lies at depth. This conclusion comes from the following analysis. We have fitted data that he had converted to an equivalent radius, R', at the surface via Eq. 11 (Fig. 8) to an $(R)^{-4}$ form. Plotting the value of Ψ at $R' = 25\,\mu m$

vs depth (Fig. 9), we see that $\Psi(R')$ increases with depth. Since the pressure effect has been taken into account by referring the radius to the surface, the increase in $\Psi(R')$ with depth means an increase of the mass of gas with depth, indicating a generation of gas at depth.

Although there does not seem to be a depth dependence in $\Psi(R)$ (see Fig. 4), possibly due to the balancing effects of the pressure effects [Eq. 11] and the positive gradient of the mass of the gas, there is a pronounced diurnal effect, which would be expected in photosynthetic activity. The model that best fits this data is:

$$\Psi_{Ph}(R, t) = C_3 t R^{-4} \qquad \text{[Eq. 14]}$$

where $t = 1$ during the night and 2 during the day. $C_3 = 1.6 \times 10^9$, but must vary considerably from location to location. In particular, away from coastal areas, C_3 might be much lower, and Eq. 14 may even take on a different form.

4.4 "Surface Emission" Bubble Concentration, Ψ_{SE}

From the discussion of Ψ_W, it was concluded that the excess of Ψ as measured by B & W would be accounted for by Ψ_{SE}. It is quite possible that these bubbles are due to a strong depth dependence for small bubbles and not due to "surface emission". However, at this stage there is no way to distinguish the process; so, for convenience, we are including them here. In addition, there is no depth information. Since we expect these bubbles to exist only near the surface, we will make an exponential dependence. Although this is quite arbitrary, to be consistent with Glotov, we need to have essentially no bubbles at his depth of measurements of 1.5 m. We therefore write

$$\Psi_{SE} = C_4 W^3 \left(1 - e^{-\frac{d_1}{d}}\right) R^{-5} \qquad 35\,\mu m < R < 80\,\mu m \qquad \text{[Eq. 15]}$$

with $C_4 = 2.7 \times 10^{11}$, chosen so that $\Psi_{SE} = \Psi_W$ at 80 μm at 0.1 m depth. $d = 0.03$ is chosen from the comments of McIntyre (1972).

CONCLUSIONS

Vertical velocity predictions seem to be fairly well established, although there may be some uncertainty due to the surface coatings of the bubbles. Lifetimes and growth predictions may be applicable for small, clean bubbles, but large uncertainties arise when the bubble has a film or coating, and when the radius of the bubble is greater than about 80 micrometres. The bubble concentration spectrum, (the number of bubbles per cubic metre per micrometre radius increment) is written as:

$$\Psi = \Psi_W + \Psi_P + \Psi_{Ph} + \Psi_{SS} + \Psi_B + \Psi_C + \Psi_{SE},$$

where the subscripts W, P, Ph, SS, B, C and SE refer to the bubble-generating mechanisms of waves, precipitation, photosynthesis, supersaturation, biological, chemical decomposition and "surface emission", respectively. Due to scarcity of data, we have attempted to model only Ψ_W, Ψ_{Ph} and Ψ_{SE}, and we must expect only rough correspondence between these models and actual data. From one observation, it appears that Ψ_C may be very small, and negligible near the surface. It is possible that Ψ_{SS}, production of gas due to heating of supersaturated water, on the other hand, may be important, but we have no information regarding this mechanism. Information of the wind dependence of Ψ_W is scant but very important to predicting Ψ. Certainly the most important aspect to be studied in the future is this wind dependence.

PART 2 BUBBLES CONTAINED IN LIVING ORGANISMS

INTRODUCTION

Since free bubbles have been discussed in some detail, it is now necessary to review the other class of bubble population in the sea — those associated with living organisms. Since the discovery of the deep scattering layer (DSL) in the 1940's [Hersey and Backus, 1962], its cause has been examined by many workers and the conclusions reached showed that it was of biological origin. Marshal [as outlined in Hersey and Backus, 1962] listed the requirements for a living organism to be responsible for the DSL — a widely distributed organism, powers of diurnal migration, sufficient concentration, and the ability to reflect sound. Two types of organisms have been shown to qualify: myctophids (also called lantern fish) [Hersey and Backus, 1962] and siphonophores (a colony of jellyfish) [Barham 1963]. The sound scattering ability of these organisms comes from associated gas bubbles that resonate at acoustic frequencies. Other hard shelled organisms have been proposed but are not discussed here since they do not contain gas bubbles.

Historically, this subject has been reviewed by Hersey and Backus [1962] in volume 1 of The Sea, a theoretical article by Weston [1967] and, most recently, by many authors in a symposium held in 1970 [Farquhar, 1970] entitled "Biological Sound Scattering in the Ocean".

In this part it is proposed to discuss the two principal types of animals involved in sound scattering and put forward some relations that may be used to model their size and distribution.

1. MYCTOPHIDS

The greater number of articles discussing this problem refer to myctophids as the main component of the DSL [Dietz, 1962; Backus et al, 1968; Batzler and Pickwell, 1970] — these are fish with lengths of 2 to 20 cm containing a gas bladder in the shape of a prolate spheroid. Marshall [1970] has studied the biology of these fish in great detail. The bladder is believed to be used to aid in the diurnal migration of the fish but its exact mode is yet to be determined [Alexander, 1970; D'Aoust, 1970]. Some fish appear to use it in the "passive" mode in which as the fish ascends or descends, the bubble expands or contracts following the gas law. The fish is believed to be in equilibrium at its upper depth limit and must expend energy at its lower limit to maintain a constant level. The other mode of operation is the "active" one in which the fish maintains the bladder at constant size during migration, creating or absorbing gas as required. Both types of operation have been inferred from acoustic results and the resolution of the problem is still an open question. For modelling purposes, the size of the swimbladder is important, along with the density of the fish population. The size of the swimbladder as related to the size of the fish has been the study of many and a summary of is available [Shearer, 1970]. There are various methods of determining volume [Shearer, 1970] which will not be discussed here but, in general, the end result is to try to obtain a relationship of the form

$$V = KL^n \qquad \text{[Eq. 16]}$$

where V is the volume of the swimbladder, K and n are the constants, and L is the length of the fish. An order-of-magnitude relationship is of the form with $K = 5 \times 10^{-4}$ and $n = 3$.

Figure 10 shows the results from Shearer [1970] where the estimated swimbladder volume is plotted against the length of the fish for four different fish. The dotted lines are the lines as fitted by Shearer [1970] but it was felt after examination that they did not adequately fit the data points. A new least-squares fit was calculated for the points, using the criterion that the square of the distance from each point to the line should be minimized [instead of the ordinate distance squared that Shearer (1970) used.] It can be seen from Fig. 10 that a steeper slope resulted without a consistent value, but was certainly higher than the commonly used 3. We tested further data from Holliday (1972] and the results can be seen in Fig. 11. The data here were in the form of histogram distributions of number of fish with given lengths and other distributions of bubble size. We assumed a one-to-one correspondence between smaller fish and smaller bubble volume to get the points on the figure — deviations from this assumption would tend to give a steeper slope. The conclusion reaches is that different values of K and n need to be used for different species, but almost all values of n were greater than 3.

As for the observed size distribution of scatterers of the myctophid type, Van Schulyer [1970] reported on this for both day and night time observations north of Hawaii. He calculated the effective radius of swimbladder and the number of scatterers per cubic metre reported, with the numbers varying from 3×10^{-3} to $3 \times 10^{-8}/m^3$. We converted these data to the same units as reported for free bubbles (number of bubbles/m^3 in a one micrometre bandwidth) and the results are shown in Fig. 12. It can be seen that the slope of the line is -5.5 which is about the same as that observed for free bubbles but with a much lower density of population. The day and night distributions were about the same. These were the only data that gave the size distribution, but other reports [Andreyeva, 1972; Johnson, 1973; Hersey and Backus, 1962] give values of total concentration that range from 4×10^{-4} to $2.4 \times 10^{-3}/m^3$. In schools, values of 10 to 15/m^3 have been reported with school sizes of 5 to 10 m wide by 10 to 100 m long, and being about 100 to 200 m apart.

2. SIPHONOPHORES

The other class of biological organisms that contains associated bubbles is the siphonophore, a jelly fish that contains a bubble at its apex that is used for flotation purposes [Barham, 1963; Pickwell, 1967]. The size of these bubbles vary from 0.03 to 2.51 mm^3 and it has been noted that these organisms can expel bubbles, thus being a source (Ψ_B) of free bubbles in the ocean. Populations of 0.3/m^3 have been noted [Barham, 1963] in a visual observation.

CONCLUSIONS

Resonant scattering from biological organisms is believed to be caused either by the gas bladder of myctophid fishes or the flotation bubble of siphonophores, with the greater work being concentrated on the former. No simple relationship exists to compute the volume of the bladder of fishes but rough estimates can be made from power law relationships. The density of population of fishes can vary by orders of magnitude whether or not a school is present, and there is no scheme proposed to date for this prediction.

REFERENCES AND BIBLIOGRAPHY

ALEXANDER, R. McN. Swimbladder gas secretion and energy expediture in vertical migrating fishes. In FARQUHAR, G.B. 1970: 74-85.

ALLEN, H.S. The motion of a sphere in a viscous fluid. Philosophical Magazine 50, 1900: 323-338.

ANDERSON, A.L., HARWOOD, R.J., LOVELACE, R.T. Investigation of gas in bottom sediment, ARL-TR-70-28. Applied Research Laboratories, The University of Texas at Austin, 1971.

ANDREYEVA, I.B. The nature of scatterers and frequency characteristics of sound scattering layers in the ocean. Oceanology 12(6) 1972: 818-822.

BACKUS, R.H., CRADDOCK, J.E., HAEDRICH, R.L., SHORES, D.L., TEAL, J.M., WING, A.S., MEAD, G.W. and CLARKE, W.D. Ceratoscopelus maderensis: peculiar sound-scattering layer identified with this Myctophid fish. Science 160, 1968: 991-993.

BARHAM, E.G. Siphonophores and the deep scattering layer. Science 140, 1963: 826-828.

BATZLER, W.E. and PICKWELL, G.V. Resonant acoustic scattering from gas-bladder fishes. In FARQUHAR 1970: 168-179.

BLANCHARD, D.C. and WOODCOCK, A.H. Bubble formation and modification in the sea and its meteorological significance. Tellus 9, 1957: 145-158.

BUXLEY, S., MCNEIL, J.E., MARKS, R.H. Jr. Acoustic detection of micro-bubbles and particulate matter near the sea surface, NPS 50306. Monterey, Calif., Naval Postgraduate School.

D'AOUST, B.G. Physiological constraints on vertical migration by Mesopelagic fishes. In FARGUHAR, G.B. 1970: 86-99.

DATTA, R.L., NAPIER, D.H. and NEWITT, D.M. The properties and behavior of gas bubbles formed at a circular orifice. Trans. Institution Chemical Engineers 23, 1950: 14-26.

DEVIN, C. Jr. Survey of thermal, radiation, and viscous damping of pulsating air bubbles in water. Jnl Acoustical Society America, 31, 1959: 1654-1667.

DIETZ, R.S. The sea's deep scattering layers. Oceanography, Freeman, San Francisco, 1962.

DORSEY, N.E. Properties of Ordinary Water Substance. New York: Reinhold, 1940.

FARQUHAR, G. Bruce (ed.). Proceedings of an International Symposium on Biological Sound Scattering in the Ocean. MC Report 005. Washington D.C., U.S. Govt. Printing Office, 1970.

FEIN, M. and MANGULIS, V. The acoustic pressure scattered by a finite number of bubbles. TRG, Inc. Report No. 023-TN-66-26, Melville N.Y. 1966.

FITZGERALD, James. Statistical study of sound speed in the inhomogeneous upper ocean, M.S. thesis. Monterey, Calif., Naval Postgraduate School, 1972.

GARRETTSON, G.A. Bubble transport theory with application to the upper ocean. Jnl Fluid Mechanics 59, 1973: 187-206. [Also Naval Postgraduate School, 6 April 1973, AD 761999].

GAVRILOV, L.R. On the size distribution of gas bubbles in water. Soviet Physics-Acoustics 15, 1969: 22-24.

GIBSON, F.W. Measurement of the effect of air on the speed of sound in water. Jnl Acoustical Society America, 48, 1970: 1195-1197.

GLOTOV, V.P., KOLOBAEV, P.A., NEUIMIN, G.G. Investigation of the scattering of sound by bubbles generated by an artificial wind in sea water and the statistical distribution of bubble sizes. Soviet Physics Acoustics 7, 1962: 341-345.

GLOTOV, V.P. and LYSONOV, Y.P. Influence of a nonuniform distribution of air bubbles on the reflection of sound from the surface layer of the ocean. Soviet Physics Acoustics 11, 1966.

GOLDSTEIN, S. Modern Developments in Fluid Dynamics, Vol 1. Oxford, The University Press, 1938: p.14.

HARTUNIAN, R.A. and SEARS, W.R. On the instability of small gas bubbles moving uniformly in various liquids. Jnl Fluid Mechanics 3, 1957: 27-47.

HERSEY, J.B. and BACKUS, R.H. Sound scattering by marine organisms. In HILL, M.N. The Sea, New York, Interscience, 1962.

HIESTAND, F.H. Bubble distributions in the upper ocean. Monterey, Calif., Naval Postgraduate School, 1971. [AD 738968].

HOLLIDAY, D.V. Resonance structure in echoes from schooled pelagic fish. Jnl Acoustical Society America 51, 1972: 1322-1332.

JOHNSON, R. Frequency dependence of the daily pattern of sea reverberation. Jnl Acoustical Society America 54, 1973: 478-482.

KELLER, D.G. Evaluation of a standing wave system for determining the presence and acoustic effect of microbubbles near the sea surface, M.S. thesis. Monterey, Calif., Naval Postgraduate School, 1968.

LAFOND, E.C. and DILL R.F. Do invisible bubbles exist in the sea. Tech. Memo. TM-259. San Diego, Calif., U.S. Navy Electronics Lab., 1957.

LEBLOND, P.H. Gas diffusion from ascending gas bubbles. Jnl Fluid Mechanics 35, 1969: 711-719.

LEIBERMAN, L. Air bubbles in water. Jnl Applied Physics 28, 1957.

MACINTYRE, F. Flow patterns in breaking bubbles. Jnl Geophysical Research 77, 1972: 5211-5228.

MACINTYRE, F. The top millimeter of the ocean. Scientific American 230, 1974: 62-77.

MARSHALL, N.B. Swimbladder development and the life of deep sea fishes. In FARQUHAR, G.B. 1970: 69-73.

MCCARTNEY, B.S. and BARRY, B.M. Echosounding on probable gas bubbles from the bottom of Saanich Inlet, British Columbia. Deep Sea Research 12, 1965: 285-294.

MEDWIN, H. In-situ acoustic measurements of bubble populations in coastal ocean waters. Jnl Geophysical Research 75, 1970: 599-611.

MEDWIN, H. The rough surface and bubble effect on sound propagation in surface ducts. Tech. Rpt. NPS-61Md71101A. Monterey, Calif., Naval Postgraduate School, 1971.

MEDWIN, H. Sound speed dispersion and fluctuations in the upper ocean: Project Bass. NPS-61Md73101A, Monterey, Calif., Naval Postgraduate School, 1973.

MEDWIN, H. Acoustic fluctuations due to microbubbles in the near-surface ocean. Jnl Acoustical Society America 56, 1974: 1100-1104.

MEDWIN, H., FITZGERALD, J. and RAUTMANN, G. Acoustic microprobing for ocean microstructure and bubbles. Jnl Geophysical Research 80, 1975: 405-413.

PICKWELL, G.V. Siphonophores and their released bubbles as acoustic targets within the deep scattering layer. In 4th US Navy Symposium on Military Oceanography, Vol I. Washington, D.C., Naval Research Laboratory, 1967: 383-395.

RAUTMANN, R. Sound dispersion and phase fluctuations in the upper ocean. NPS-61Md72022A. Monterey, Calif., Naval Postgraduate School, 1972.

SCHULKIN, M. Surface-coupled losses in surface sound channels. Jnl Acoustical Society America 44, 1968: 1152-1154.

SCHULKIN, M. Surface-coupled losses in surface sound channel propagation. II. Jnl Acoustical Society America 45, 1969: 1054-1055.

SCHULKIN, M. The propagation of sound in imperfect ocean surface ducts. U.S.L. Report No. 1013. New London, Conn., U.S. Navy Underwater Sound Laboratory, 1969.

SHEARER, L.W. Comparisons between surface-measured swimbladder volumes, depth of resonance and 12 kHz echograms at the time of capture of sound-scattering fishes. In FARQUHAR, G.B. 1970: 453-473.

TOBA, Y. and KUNISHI, H. Breaking of wind waves and the sea surface wind stress. Jnl Oceanographical Society of Japan 26, 1970: 71-80.

TURNER, J.S. Buoyancy effects in fluids. Cambridge, The University Press, 1973: 474-481.

TURNER, W.R. Microbubble persistence in fresh water. Jnl Acoustical Society America 33, 1961: 1223-1232.

URICK, R.J. and HOOVER, R.M. Backscattering of sound from the sea surface: its measurement, causes, and application to the prediction of reverberation levels. Jnl Acoustical Society America 28, 1956: 1038-1042.

VAJDA, T.C. Bubble distributions in a quiescent ocean calculated from the bubble transport equation. Monterey, Calif., Naval Postgraduate School, 1972. [AD 749046].

VAN SCHULYER, P. An acoustically determined distribution of resonant scattering north of Oahu. In FARQUHAR, G.B. 1970: 328-340.

WANG, P.C.C. and MEDWIN, H. Statistical considerations to experiments on the scattering of sound by bubbles in the upper ocean. NPS-53Wg72101A, Monterey, Calif., Naval Postgraduate School, 1972.

WESTON, D.E. Underwater Acoustics, Vol 2, Ch 5. In ALBERS. V.M. (ed.) Sound propagation in the presence of bladder fishes. New York, Plenum Press, 1967.

WIENS, L.A. Development and testing of an acoustic system for in-situ determination of microbubble concentrations in the ocean. Monterey, Calif., Naval Postgraduate School, 1971. [AD 72869].

WYMAN, J. Jr., SCHOLANDER, P.F. EDWARDS, G.A. and IRVING, L. On the stability of gas bubbles in sea water. Jnl Marine Research 11, 1952: 47-62.

ZIMDAR, R.E., BARNHOUSE, P.D., and STOFFEL, M.J. Instrumentation to determine the presence and acoustic effect of microbubbles near the sea surface, M.S. thesis. Monterey, Calif., Naval Postgraduate School, 1964.

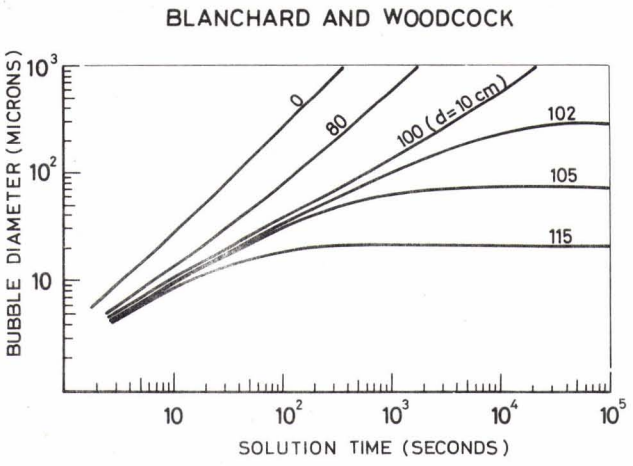

FIG. 1
BUBBLE LIFETIMES

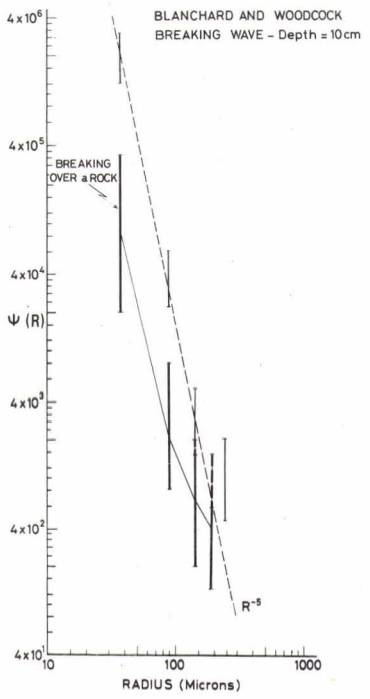

FIG. 2
BUBBLE SPECTRUM – BLANCHARD AND WOODCOCK

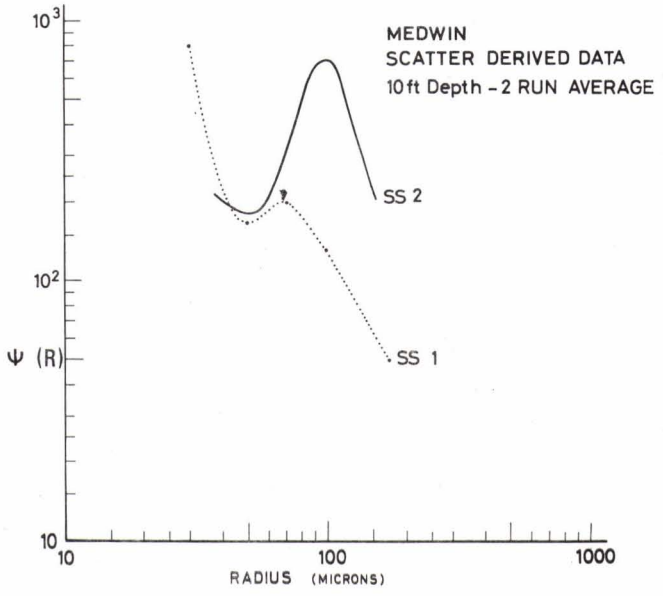

FIG. 3
BUBBLE SPECTRUM – MEDWIN

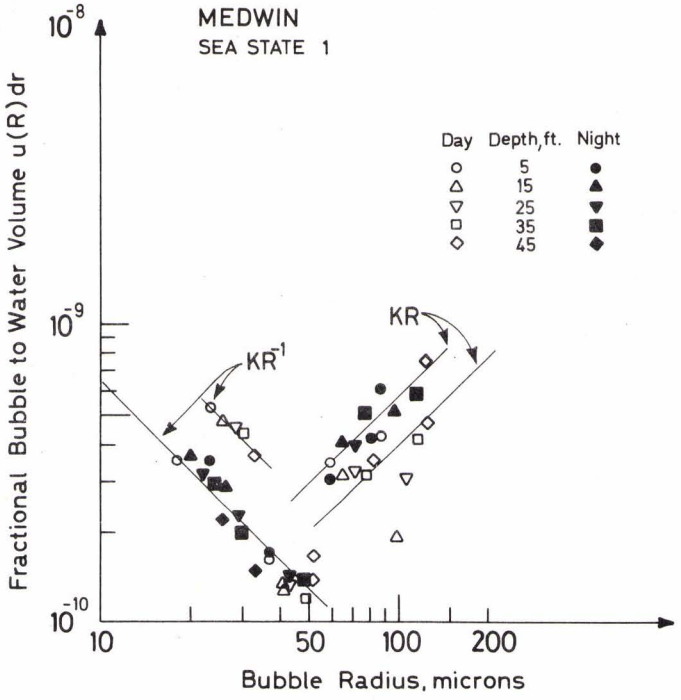

FIG. 4
'FRACTIONAL VOLUME' SPECTRUM – MEDWIN

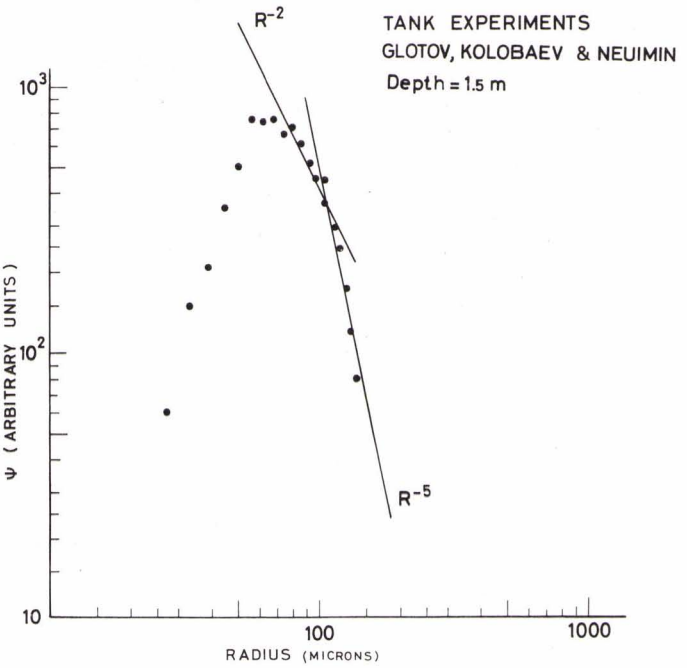

FIG. 5
BUBBLE SPECTRUM – GLOTOV

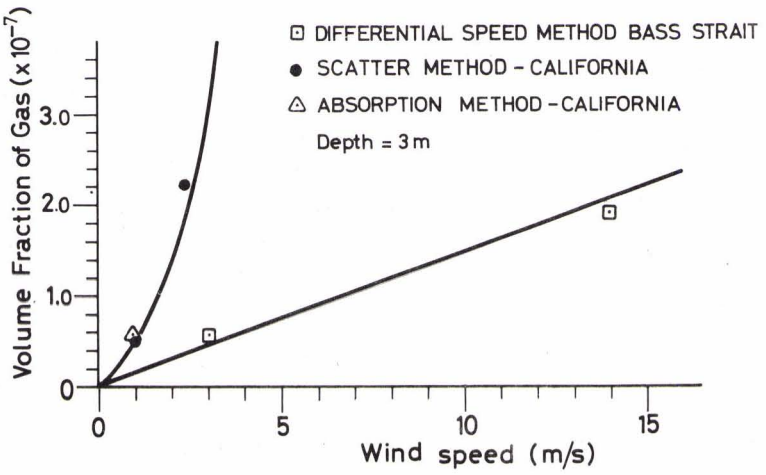

FIG. 6
BUBBLE WIND DEPENDENCE

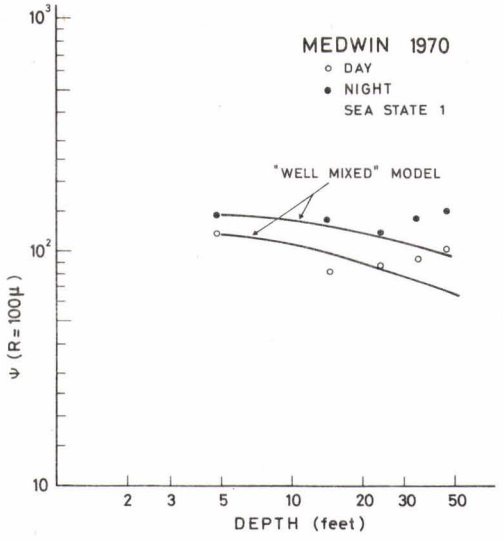

FIG. 7
BUBBLE DEPTH DEPENDENCE

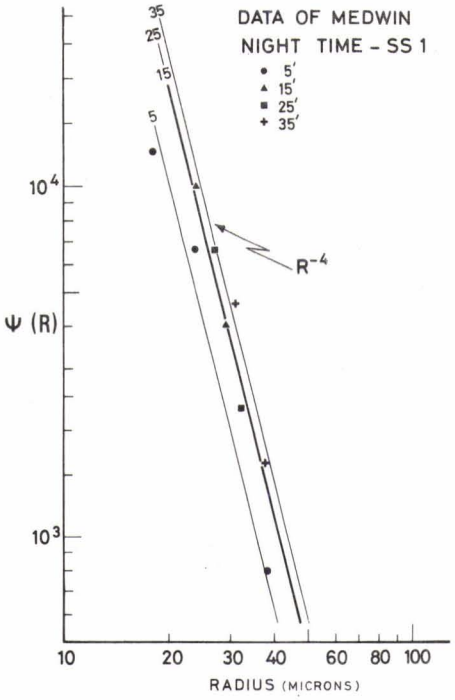

FIG. 8
ISOFREQUENCY DEPTH DEPENDENCE

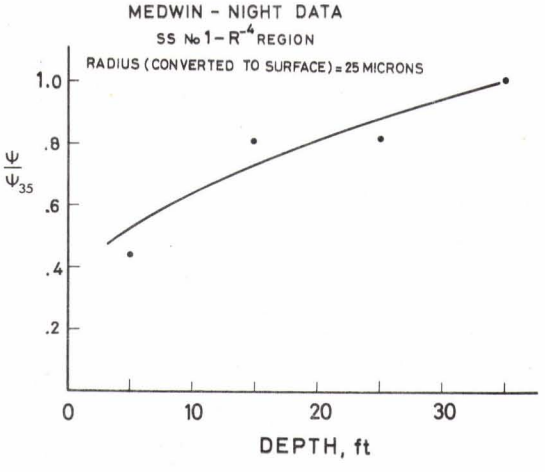

FIG. 9
DEPTH DEPENDENCE AT CONSTANT RADIUS

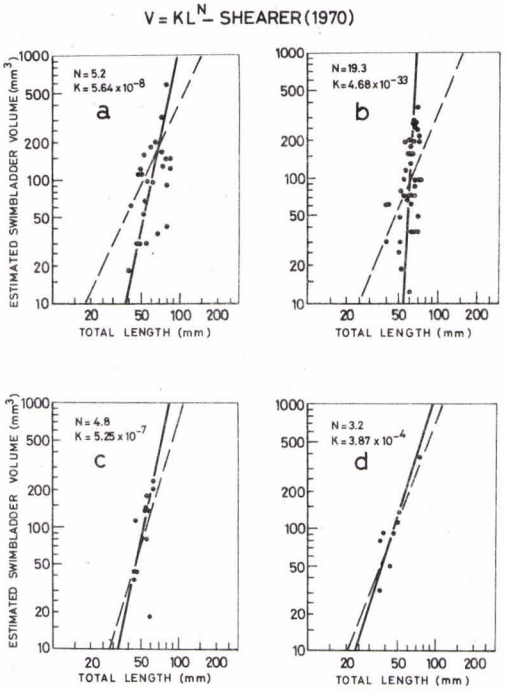

FIG. 10
ESTIMATED SWIMBLADDER VOLUME – VS FISH LENGTH
a Myctophum Nitidulum (surface)
b Lepidophanes Güntheri 0 – 230 m
c Diaphus Brachycephalus 230 – 0 m
d Sternoptyx Diaphana 860 – 0 m

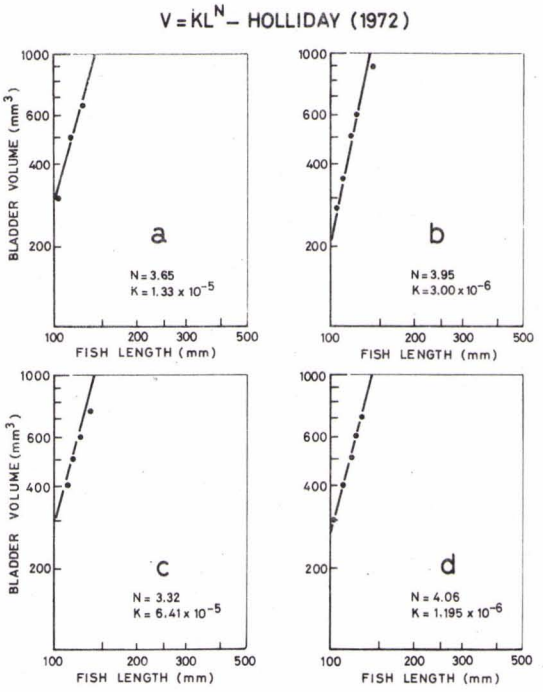

FIG. 11
ESTIMATED SWIMBLADDER VOLUME – VS FISH LENGTH
Anchovy

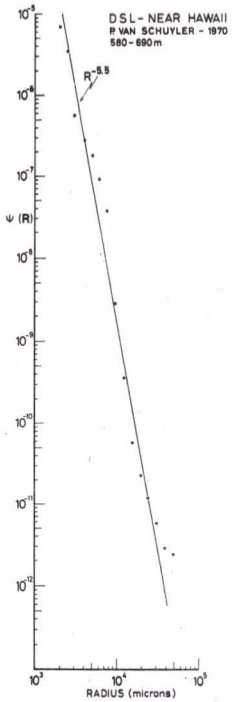

FIG. 12
BUBBLE SPECTRUM FOR A DEEP SCATTERING LAYER

ACOUSTICAL PROBING FOR MICROBUBBLES AT SEA

by

Herman Medwin
Department of Physics and Chemistry
Naval Postgraduate School
Monterey, California 93940
U.S.A.

ABSTRACT

Free gas bubbles have been indicted for many physical processes at sea including: scavenging detritus and chemicals from the ocean volume; generating droplets whose salts affect thunderstorm activity over the sea; providing cavitation nuclei; producing sound scatter and sound attenuation. It is the latter two phenomena that make acoustic measurements the most promising pathway for conducting a census of bubble populations. In particular, the very large scattering and extinction cross sections of a bubble at resonance, and the dispersion of sound speed in bubbly water, have made it possible to recently obtain marine bubble populations as a function of radius from 20 to 300 microns at depths to 15 metres. The growing knowledge of bubble numbers and behaviour will, in turn, permit more accurate predictions of sound propagation and fluctuations, particularly near the sea surface.

1. Review of Bubble Theory

1.1 Single Bubbles

Acousticians know very well that when a gas bubble in water senses a frequency at or near its natural frequency it will very effectively absorb and scatter that sound. At resonance, the scattering and absorption cross-sections of a typical bubble at sea are of the order 1000 times its geometrical cross-section and 10^8 times the scattering cross-section of a rigid sphere of the same radius. See Figure 1.1

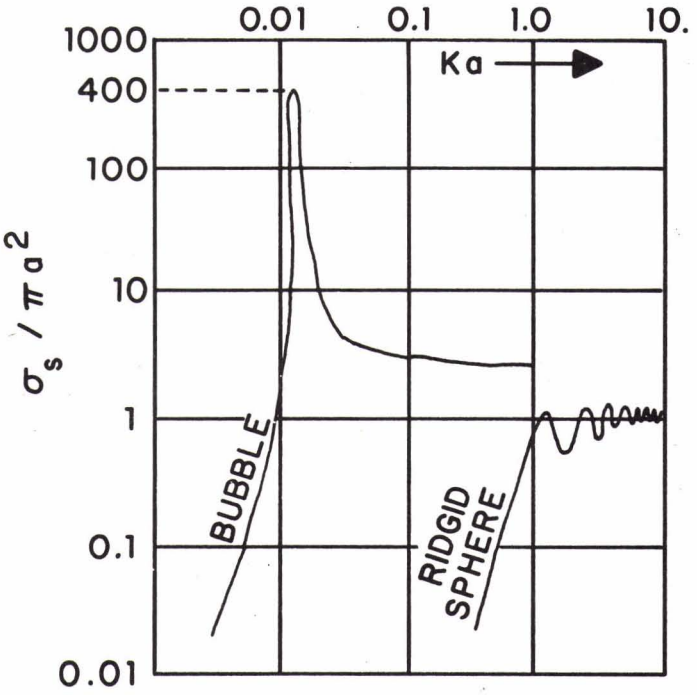

FIG. 1.1
RATIO OF SCATTERING CROSS SECTION, σ_s, TO GEOMETRICAL CROSS SECTION FOR BUBBLE AND RIGID SPHERE. k IS WAVE NUMBER IN WATER

Our first need is to review the behavior of single bubbles in order to determine the effect of the bubble parameters on the resonance frequency, damping constants and acoustical cross sections. We will then consider the propagation of sound in bubbly water.

To calculate the natural body frequency at which a bubble resonates, assume for simplicity that the motion of the bubble is completely accounted for by two factors: a) the compressibility of the enclosed gas during reversible expansion and compression with no heat exchange (adiabatic oscillation); and b) the liquid mass moved by the bubble as it oscillates. For the present we will assume that the damping is negligible and that there are no effects due to surface tension or thermal conductivity.

a) Bubble Stiffness: Start with the adiabatic gas relation, pV^{γ} = constant where p is the instantaneous total pressure within the bubble volume, V. The constant, γ, is the ratio of specific heats for the enclosed gas. Differentiating yields

$$\frac{P_i}{dV} = \frac{\gamma P_o}{V}$$

where P_i, the instantaneous incremental pressure is $p - P_o$; P_o is ambient pressure ($P_o >> |p_i|$); dV is incremental volume.

The stiffness restoring force acting over the entire spherical surface is

$$F_r = 4\pi a^2 p_i = - (12\pi\gamma P_o a)\xi \qquad (1.1.1)$$

Equation (1.1.1) is in the form of Hooke's Law where a is the average radius of the bubble. The quantity in parentheses is the stiffness constant, s_A; the subscript, A, refers to adiabatic and other assumptions.

$$s_A = 12\pi\gamma P_o a \qquad (1.1.2)$$

b) Bubble Mass: The major part of the oscillating mass is due to the liquid adjacent to the bubble rather than the mass of the gas. The inertial force acting over the bubble surface is determined by calculating the pressure of the reradiated sound. Later we will verify that, at resonance, $ka << 1$, where k is the wave number in water, and that the scattered pressure wave is therefore isotropic and is given by

$$\underset{\sim}{p_s} = \frac{\sqrt{2}\, P_{\dot{m}S}}{R} \exp\,[i(\omega t - kR)] \qquad (1.1.3)$$

where $\underset{\sim}{P}_s$ is the rms scattered pressure at 1 m radius.

The acoustic momentum equation in spherical coordinates has the radial component

$$\rho \ddot{\xi} = - \frac{\partial p_s}{\partial R}$$

where ρ is water density. At the bubble surface

$$\rho \ddot{\xi}\Big]_{R=a} = \frac{\sqrt{2}\,\underset{\sim}{P}_s}{R^2}(1-ikR)e^{i(\omega t-kR)}\Big]_{R=a}$$

Since $ka << 1$ this simplifies to

$$|p_s| = \rho\, a\, |\ddot{\xi}| \qquad (1.1.4)$$

The equivalent mass is found by calculating the inertial force at the surface

$$F_m\Big]_{R=a} = - p_s\Big]_{R=a}(4\pi a^2)$$

$$= - 4\pi\, {}^3\rho\, \ddot{\xi}\Big]_{R=a} \qquad (1.1.5)$$

Equation (1.1.5) allows us to identify an effective mass of water

$$m = 4\pi a^3 \rho \qquad (1.1.6)$$

that rides with the bubble as it oscillates at low frequencies, $ka << 1$.

Newton's Second Law is therefore

$$F_r = ma$$

$$\underbrace{- 12\pi\gamma P_o a\xi}_{S_A} = \underbrace{4\pi a^3 \rho}_{m}\ddot{\xi} \qquad (1.1.7)$$

The natural frequency of the free oscillation, f_{RA}, depends only on the constants of the system,

$$f_{RA} = \frac{1}{2\pi}\sqrt{\frac{S_A}{m}} = \frac{1}{2\pi a}\sqrt{\frac{3\gamma P_o}{\rho}} \qquad (1.1.8)$$

The subscript, R, refers to resonance and, A, refers to the mentioned assumption. For an air bubble assumptions in water at sea level pressure this simplifies to

$$f_{RA} = \frac{3.25}{a(\text{meters})} = \frac{3.25 \times 10^6}{a(\text{microns})} \qquad (1.1.9)$$

Defining k_R, the wave number in water at the resonance frequency, the sea level value of $k_R a$ is 0.0136 for an air bubble. This verifies the assumption, $k_R a \ll 1$.

For bubbles of small radii, surface tension becomes a significant additional restoring force. Furthermore, the assumption that the gas vibrates adiabatically is no longer valid if the bubble radius is very small; then the oscillation is more nearly isothermal. When these points are considered, the equation for the resonance frequency changes. P_o in (1.1.8) is replaced by the average interior pressure including surface tension, $P_{io} = \beta P_o$, and γ is replaced by the effective ratio of specific heats in the presence of thermal conductivity γb.
The generalization is

$$f_R = \frac{1}{2\pi a}\sqrt{\frac{3\gamma b \beta P_o}{\rho}} = f_{RA}(\beta b)^{1/2} \qquad (1.1.10)$$

The detailed expressions for b and β will be given later. Figure 1.2 shows their behavior for air bubbles at sea level.

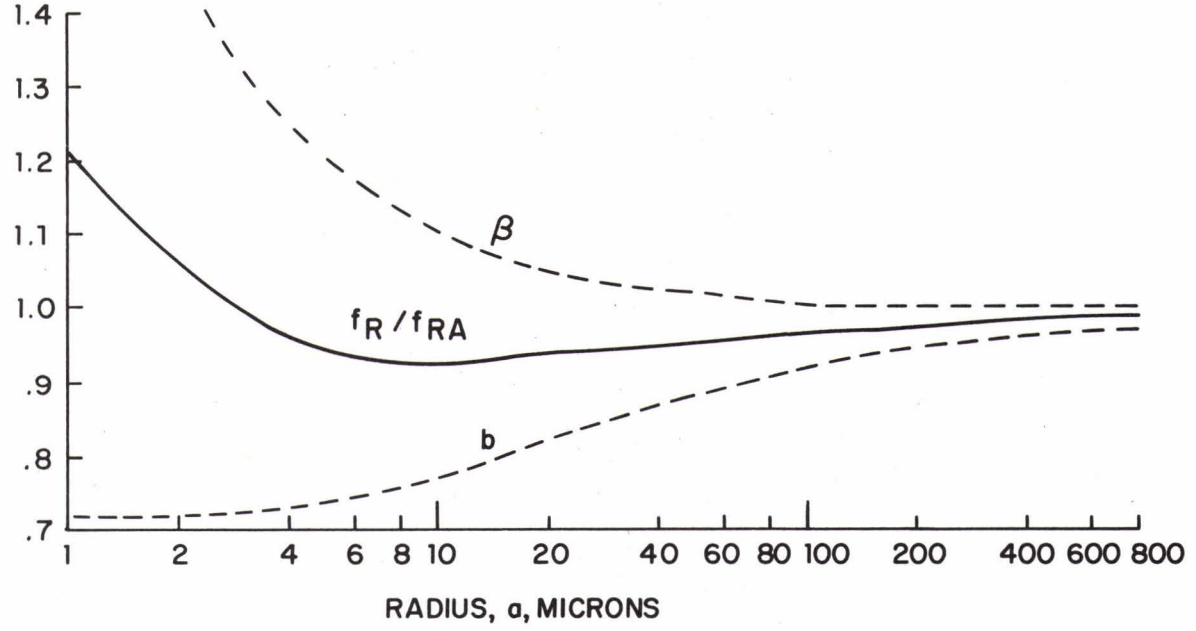

FIG. 1.2
CORRECTIONS TO Eq. 1.1.8 FOR CALCULATION OF BUBBLE RESONANCE FREQUENCY. β AND b ARE GIVEN BY Eqs. (1.1.31) AND (1.1.32) AND ARE PRINCIPALLY FUNCTIONS OF SURFACE TENSION AND THERMAL CONDUCTIVITY, RESPECTIVELY.

The surface tension correction, β, differs from unity by less than 1% for bubbles of radius 100 microns or greater. The thermal conductivity parameter, b, approaches the isothermal value, $1/\gamma$, for very small bubbles and unity for large ones. Fig 1.2 shows that the two effects are to some extent mutually counteracting in their effect on the resonance frequency of bubbles greater than 2 microns, so that the simpler equation (1.1.8) is at worst 8% in error for this case.

1.1.2 Scattering cross section and damping constants

Assume that the bubble is irradiated by a sound field of wave length much greater than the bubble radius ($ka << 1$). The incident plane wave is therefore uniform at all points of the bubble.

$$\underset{\sim}{p}_P = \sqrt{2}\underset{\sim}{P}_P e^{i\omega t} \tag{1.1.11}$$

Where $\underset{\sim}{P}_p$ is the rms incident plane wave pressure. The incident intensity is

$$I_p = \frac{|P_p|^2}{\rho c} \tag{1.1.12}$$

From (1.1.3) the scattered intensity is

$$I_S = \frac{|P_S|^2}{R^2 \rho c} \tag{1.1.13}$$

The scattering cross section is the ratio of the scattered power to the incident intensity,

$$\sigma_s = \frac{\int_A I_S dA}{I_P} = \frac{4\pi R^2 \dfrac{|P_S|^2}{R^2 \rho c}}{\dfrac{|P_P|^2}{\rho c}} = 4\pi \frac{|P_S|^2}{|P_P|^2} \tag{1.1.14}$$

To determine the pressure ratio in eq (1.1.14) express the pressure and particle velocity boundary conditions at the bubble surface. Denote the interior acoustic pressure by

$$\underset{\sim}{p}_i = \sqrt{2}\underset{\sim}{P}_i e^{i\omega t} \tag{1.1.15}$$

where $\underset{\sim}{P}_i$ is the rms interior pressure.

In addition to the pressures given by Eqs (1.1.3), (1.1.11) and (1.1.15) we must add a shear viscous stress proportional to the radial rate of strain, u_r/R at the surface. The proportionality constant, $C_1\mu$, includes the dynamic coefficient of shear viscosity for water, μ, and the dimensionless constant, C_1, which depends on the geometry.

The boundary condition for pressure is

$$p_i = p_p + p_s + C_1\mu \left.\frac{u_r}{R}\right]_{R=a} \tag{1.1.16}$$

To obtain u_r in terms of the scattered pressure use the radial component of the acoustic force equation at the surface,

$$\rho \left.\frac{\partial u_r}{\partial t}\right]_{R=a} = -\left.\frac{\partial p_s}{\partial R}\right]_{R=a}$$

Assuming harmonic time dependence for u_r,

$$\underset{\sim}{u}_r = \frac{-i\sqrt{2}\,\underset{\sim}{P}_S\, e^{i\omega t}}{\rho c k a^2} \tag{1.1.17}$$

To obtain p_s at R = a expand the exponential in Eq (1.1.3),

$$\underset{\sim}{P}_S = \frac{\sqrt{2}\,\underset{\sim}{P}_S}{a}\, e^{i\omega t}(1-ika) \tag{1.1.18}$$

Inserting these results into (1.1.16), the pressure condition at R = a is

$$\underset{\sim}{P}_i = \underset{\sim}{P}_P + \frac{\underset{\sim}{P}_S}{a}(1 - ika) - \frac{i\mu C_1 \underset{\sim}{P}_S}{\rho c k a^3} \tag{1.1.19}$$

Next turn to the velocity condition. The interior radial particle velocity at the surface can be evaluated in terms of the alternating pressure, $\underset{\sim}{p}_i$. First, consider the relation between the bubble volume and the interior pressure.

For small bubbles the effective value of the ratio of specific heats, γ, approaches unity. Of equal importance, the interior bubble pressure and temperature do not instantly follow the volume variation. Therefore, rewrite the adiabatic law to allow the magnitude of the exponent and the phase between pressure and volume to be functions of driving frequency and bubble size,

$$\underset{\sim}{p}_{iT} \, V^{\gamma(b+id)} = \text{constant} \tag{1.1.20}$$

where

$$\underset{\sim}{p}_{iT} = P_{io} + \underset{\sim}{p}_{i} = \text{total interior pressure.} \tag{1.1.21}$$

b and d are real dimensionless numbers. Differentiate with respect to time, use

$$\frac{d\underset{\sim}{V}}{dt} = 4\pi a^2 \, \underset{\sim}{u}_r \Big]_{R=a} \tag{1.1.22}$$

and

$$u_r \Big]_{R=a} = \frac{-i\omega a \sqrt{2} \, P_i \, e^{i\omega t}}{3\gamma(b+id) P_{io}} \tag{1.1.23}$$

Equate to the particle velocity of the radiated wave at R = a, given by (1.1.17), rearrange to

$$\frac{\underset{\sim}{P}_i}{\underset{\sim}{P}_S} = \frac{3\gamma(b+id) P_{io}}{\rho c^2 k^2 a^3} \tag{1.1.24}$$

which, with the aid of (1.1.10), can be written

$$\frac{\underset{\sim}{P}_i}{\underset{\sim}{P}_S} = \frac{1}{a}\left(\frac{f_R}{f}\right)^2\left(1 + id/b\right) \tag{1.1.25}$$

Also, since eqs (1.1.17) and (1.1.23) show that $\underset{\sim}{u}_r$ lags $\underset{\sim}{p}_s$ by 90° and leads $\underset{\sim}{p}_P$ by 90°, when evaluated at R = a and f << f_R, we replace $\underset{\sim}{P}_p$ by - P_p. This effectively fixes the phase in terms of the incident wave as reference. Then

$$\frac{\underset{\sim}{P}_S}{P_P} = \frac{-a}{\left[\left(\frac{f_R}{f}\right)^2 - 1\right] + i\left[ka + \left(\frac{d}{b}\right)\left(\frac{f_R}{f}\right)^2 + \frac{C_1\mu}{\rho\omega a^2}\right]} \tag{1.1.26}$$

Now define the damping constants

$$\delta = \delta_r + \delta_t + \delta_v \tag{1.1.27}$$

where

δ_r = ka is the damping constant due to reradiation;

$\delta_t = (d/b)(f_R/f)^2$ is the damping constant due to thermal conductivity;

and $\delta_v = \frac{4\mu}{\rho\omega a^2}$ is the damping constant due to shear viscosity.

Our proportionality constant C_1 has been given the value 4, as found in other studies (Devin 1959).

The scattering cross section is obtained by inserting (1.1.26) into (1.1.14)

$$\sigma_S = 4\pi\frac{\underset{\sim}{P}_S\underset{\sim}{P}_S^*}{P_P} = \frac{4\pi a^2}{\left[\left(\frac{f_R}{f}\right)^2 - 1\right]^2 + \delta^2} \tag{1.1.28}$$

It is clear that at resonance the values of δ are crucial to the size of the scattering cross section. The damping constants have been evaluated in terms of the physical constants of the gas bubble and water. (Ref. Eller, A.I. (1970) and Devin, C. (1959)). In referring to the above articles note that Devin is principally concerned with the damping constants at resonance and that Eller's damping constants are related to ours by $d(\text{eller}) = \delta(f/f_R)^2$.

In order to obtain δ_t, the thermal damping constant, calculate

$$d/b = 3(\gamma-1)\left[\frac{X(\sinh X + \sin X) - 2(\cosh X - \cos X)}{X^2(\cosh X - \cos X) + 3(\gamma-1)X(\sinh X - \sin X)}\right], \quad (1.1.29)$$

where

$$X = a\left(\frac{2\omega\rho_g C_{Pg}}{K_g}\right)^{1/2} \quad (1.1.30)$$

The constants needed for the resonance frequency equation, (1.1.10), are

$$\beta = P_{io}/P_o = 1 + \frac{2\tau}{P_o a}\left(1 - \frac{1}{3\gamma b}\right) \quad (1.1.31)$$

and

$$b = \left[1 + (d/b)^2\right]^{-1}\left[1 + \frac{3(\gamma-1)}{X}\left(\frac{\sinh X - \sin X}{\cosh X - \cos X}\right)\right]^{-1} \quad (1.1.32)$$

In summary, to calculate the resonance frequency and the damping constants, the procedure is: Obtain the physical constants of the bubble at the depth, Z ; this will include the constants of the gas, ρ_{gO}, K_g, C_{pg}, γ, the constants of the water, ρ ,μ and the surface tension between them, τ. For a given sound frequency and bubble radius calculate X, and then d/b, b and β in that order. The resonance frequency for that bubble radius can then be obtained from eq (1.1.10) and the damping

constants readily fall out of equations (1.1.27). The damping constants at resonance are shown in Fig 1.3

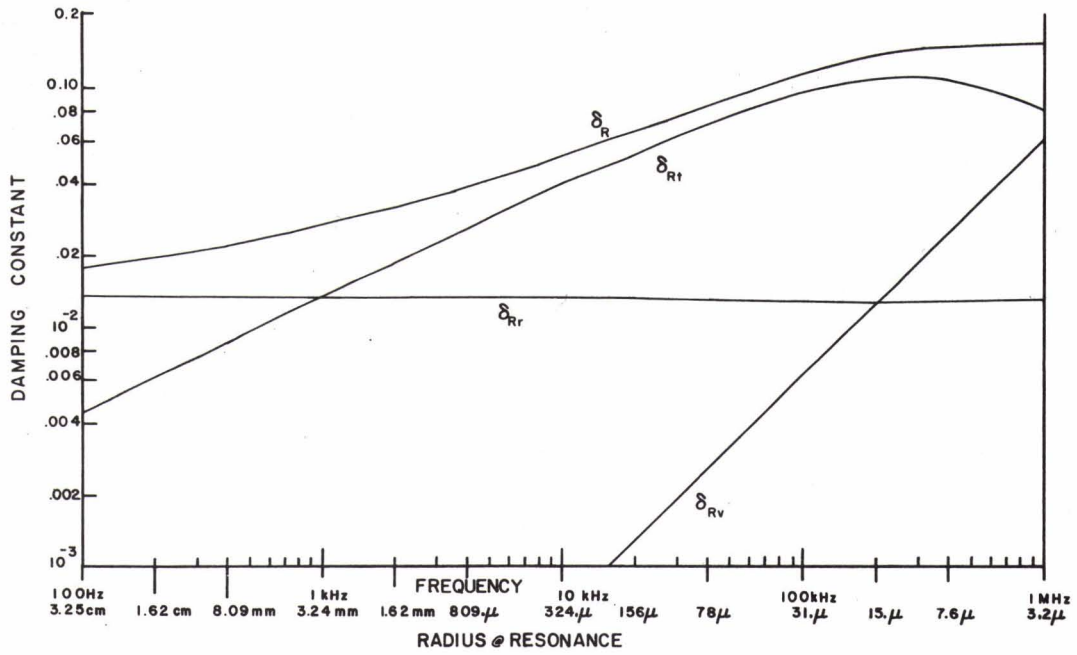

FIG. 1.3
DAMPING CONSTANTS AT RESONANCE, δ_{Rt}, δ_{RV} AND δ_{Rr} ARE COMPONENTS DUE TO THERMAL CONDUCTIVITY, SHEAR VISCOSITY AND SCATTER

In order to calculate the acoustical cross sections it is necessary, also to look at the damping constants off-resonance. Fig 1.4 shows the damping constants of bubbles as a function of radius at frequencies 1, 10, 100 kHz. The resonance radius, a_R, is indicated. Fig 1.4 (next page) shows that the damping constant for a given sound frequency is dominated by different mechanisms depending on the bubble radius. For $a >> a_R$, δ depends principally on scatter, (δ_r), and is proportional to the radius (see eq 1.1.27); bubbles near, and down to two decades smaller than, the resonance radius have damping constants largely caused by thermal conductivity; very small bubbles $a << a_R$ have large damping constants proportional to a^{-2} due solely to shear viscous losses. The minimum damping constant occurs at radius $a_{min} > a_R$; the ratio a_{min}/a_R increases with increasing frequency.

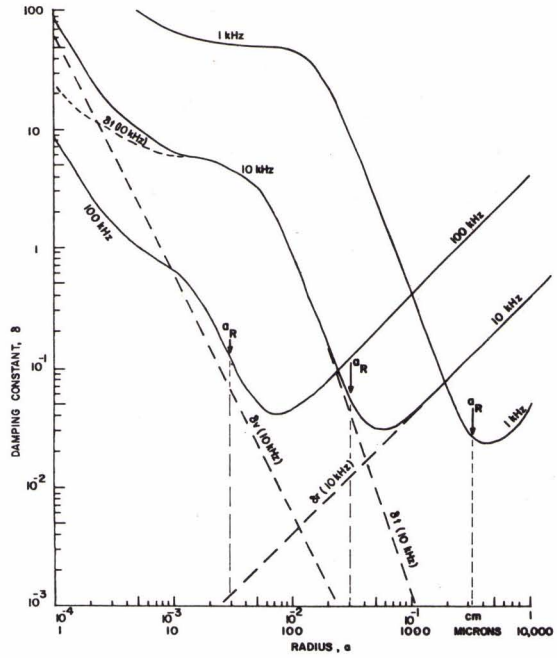

FIG. 1.4
DAMPING CONSTANTS OFF RESONANCE. RESONANCE RADII ARE INDICATED

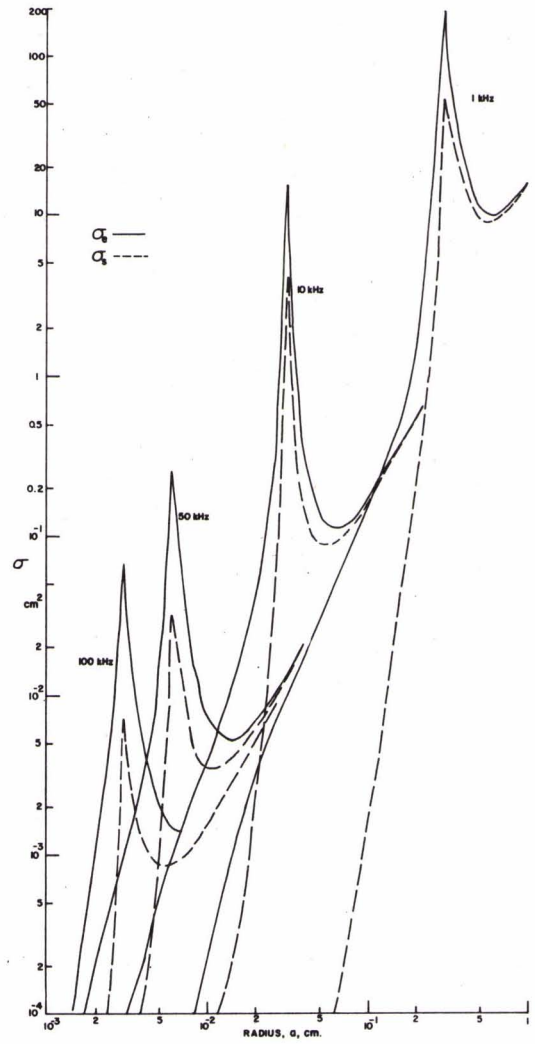

FIG. 1.5
σ_e AND σ_s FOR AIR BUBBLES AT SEA LEVEL

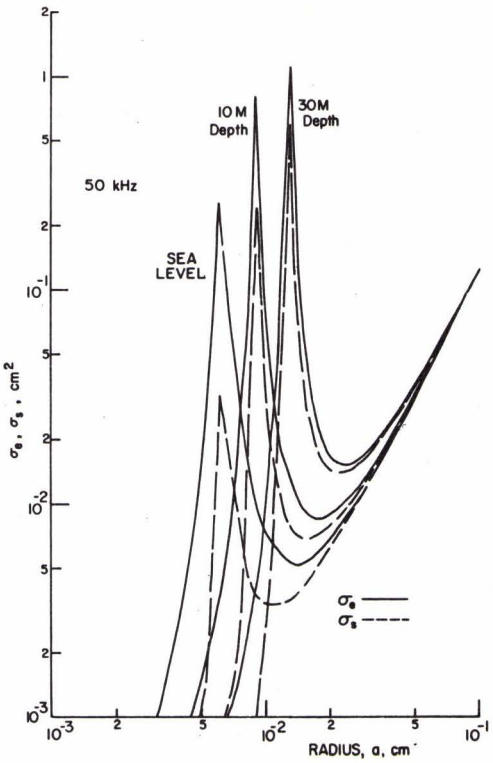

FIG. 1.6
σ_e AND σ_s FOR AIR BUBBLES AT THREE DEPTHS. f = 50 kHz

Fig 1.5 shows σ_s and σ_e as a function of bubble radius for air bubbles at sea level, ensonified by 1, 10, 50 and 100 kHz sound. In Fig 1.6 σ_s and σ_e are plotted for 50 kHz sound for bubbles at different depths. σ_e will be discussed in the next section.

1.1.3 Absorption and extinction cross sections

The extinction cross section of a bubble can be calculated from

$$\sigma_e = \Pi_e / I_p \tag{1.1.37}$$

where Π_e is obtained by integrating the product of the force by the velocity, at R = a,

$$\Pi_e = \frac{1}{T} \int_T (\underset{\sim}{p}_p)(4\pi a^2)(\underset{\sim}{\dot{\xi}})\, dt \Big]_{R=a} \tag{1.1.38}$$

We readily get

$$\sigma_e = \frac{\Pi e}{P_p^2/\rho c} = \frac{4\pi a^2 (\delta/ka)}{[(f_R/f)^2 - 1]^2 + \delta^2} \tag{1.1.39}$$

Comparison of the equations for scatter and extinction make it clear that

$$\sigma_e = \sigma_s (\delta/\delta_r) \tag{1.1.40}$$

Also, since sound extinction is composed of scatter plus absorption,

and $$\sigma_e = \sigma_s + \sigma_a, \tag{1.1.41}$$

we have

$$\sigma_a = \sigma_s \left(\frac{\delta_t + \delta_v}{\delta_r} \right) \tag{1.1.42}$$

Recall that δ_t and δ_v measure true sound absorption whereas δ_r measures scatter out of the beam. Therefore, the last two equations state that the cross sections are directly proportional to the particular damping constants that cause them.

1.2 Homogeneous Bubbly Water

1.2.1 Attenuation

a) Bubbles of one size only: Assume that we have water containing bubbles of unique radius, a, and that the bubbles are far enough apart to prevent interaction effects. Effectively this will be true when the separation is greater than $\sqrt{\sigma_e}$. If a sound beam propagates through such a medium the excess attenuation due to bubbles can be obtained by simply adding the extinction effect of each bubble. Assuming N resonant bubbles per unit volume, the change of intensity over a distance dx is

$$dI = I_p \sigma_e N(a) dx$$

The excess attenuation in decibels per unit distance due to bubbles will be

$$\alpha_b = \frac{\Delta SPL}{x} = 4.34 \sigma_e N(a) \qquad (1.2.1)$$

where the length units must be consistent, e.g.,

$$[\sigma_e] = M^2 \ , \ [N(a)] = M^{-3}, \ [\alpha] = dB/M$$

b) Bubbles of Many Sizes: At sea there will be a mixture of bubbles sizes. The total extinction cross section per unit volume, S_e, for sound traversing a random mixture of non-interaction of bubbles is calculated by integration

$$S_e = \int_0^\infty \sigma_e n(a) da = \int_\delta^\infty \frac{4\pi a^2 (\delta/\delta_r) n(a) da}{[(f_R/f)^2 - 1]^2 + \delta^2} \qquad (1.2.2)$$

where n(a) da is the number of bubbles per unit volume having a radius between a and a+ da.

When Eq 1.2.2 is integrated (Eckart 1945) by assuming that both δ_R and n(a) da are constant over the major part of the resonance peak,

$$S_e = 2\pi^2 a_R^3 \frac{n(a_R)}{\delta_{Rr}}$$

which replaces σ_e N in eq 1.2.1.

Accordingly the excess attenuation due to bubbles is estimated as

$$\alpha_b = 8.68 \ \pi^2 \ \frac{a^3_R}{\delta_{Rr}} n(a_R) = \frac{20.5 \ u(a_R)}{\delta_{Rr}} \qquad (1.2.3)$$

where u(a)da is the ratio of bubble gas volume to water volume for bubbles between radius a_R and $a_R + da_R$. That is,

$$u(a_R)da_R = [\frac{4}{3}\pi a_R^3]n(a_R)da_R$$

1.2.2 Dispersion of sound speed

a) Bubbles of One Size Only: The dependence of the sound speed on the compressibility and density is given by

$$c^2 = E/\rho = \frac{1}{\rho K}$$

where the compressibility is the reciprocal of the bulk elasticity,

$$K = \frac{1}{E} = \frac{\Delta\rho/\rho}{\Delta\rho} = \frac{|\Delta v/v|}{\Delta P} = K_o + \underset{\sim}{K}_1 \qquad (1.2.4)$$

The presence of bubbles in sea water affects the speed of sound primarily because of the changed compressibility. K_o is the part of the compressibility due to the water and $\underset{\sim}{K}_1$ is the part due to the change in volume of the bubbles. $\underset{\sim}{K}_1$ is written as a complex quantity to allow for the phase shift of volume change with respect to pressure change.

K_o is expressed in terms of the speed of sound through bubble-free water, c_o, and the density, ρ_o,

$$K_o = \frac{1}{\rho_o c_o^2} \qquad (1.2.5)$$

The compressibility due to the bubbles is found by using the displacement from eq (1.1.34) in (1.2.4)

$$\underset{\sim}{K}_1 = \frac{N\underset{\sim}{\Delta v}}{\Delta P} = \frac{NS\underset{\sim}{\xi}}{\sqrt{2}\, p_p e^{i\omega t}} = \frac{NS^2}{m\omega^2[(-1+\frac{\omega_R^2}{\omega^2})+i\frac{R_m}{\omega m}]} \qquad (1.2.6)$$

where

N is number of bubbles of radius, a, per unit volume, Δv is change in volume for each bubble, $S = 4\pi a^2$ is surface area of each bubble and $\underset{\sim}{\xi}$ is radial displacement of bubble surface. To simplify we define the frequency ratio

$$Z = f_R/f = \omega_R/\omega \qquad (1.2.7)$$

Then,

$$\underset{\sim}{K}_1 = \frac{N4\pi a[Z^2-1-i\delta]}{\rho_o\omega^2[(Z^2-1)^2+\delta^2]} \qquad (1.2.8)$$

The expression for the speed of sound in the bubbly medium is now

$$\underset{\sim}{c} = \left(\frac{1}{\rho_o \underset{\sim}{K}}\right)^{1/2} = \frac{c_o}{[1+A-iB]^{1/2}} \qquad (1.2.9)$$

where

$$A = \left(\frac{Z^2-1}{(Z^2-1)^2+\delta^2}\right)\left(\frac{4\pi a N c_o^2}{\omega^2}\right) \text{ and } B = \left(\frac{\delta}{(Z^2-1)^2+\delta^2}\right)\left(\frac{4\pi a N c_o^2}{\omega^2}\right)$$

Take the real part of $\underset{\sim}{c}$ for the dependence of the speed on the parameters of the bubbly region.

$$\mathrm{Re}\{\underset{\sim}{c}\} = c_o\left[1 - \frac{2\pi a N c_o^2}{\omega^2}\,\frac{(Z^2-1)}{(Z^2-1)^2+\delta^2}\right] \qquad (1.2.10)$$

It is useful to write the speed in terms of the fraction of gas in bubble form, U(a),

$$U(a) = [N(a)]\left[\tfrac{4}{3}\pi a^3\right] \qquad (1.2.11)$$

Then,

$$\mathrm{Re}(\underset{\sim}{c}) = c_o\left[1 - \frac{3UZ^2}{2a^2k_R^2}\,\frac{Z^2-1}{(Z^2-1)^2+\delta^2}\right] \qquad (1.2.12)$$

Where $k_R = \omega_R/c_o$

Consider the special cases for extreme frequencies. For $Z \gg 1$,

$$c_{\ell f} = c_o\left[1 - \frac{3U}{2a^2k_R^2}\right] \quad f \ll f_R, \qquad (1.2.13)$$

so that the low frequency asymptotic speed depends only on the total gas volume.

At the other extreme for $Z << 1$

$$c_{hf} = c_o \left[1 + \frac{3UZ^2}{2a^2 k_R^{\ 2} (1+\delta^2)} \right] \rightarrow c_o \quad \cdot \quad f >> f_R \tag{1.2.14}$$

Therefore bubbles do not affect the sound phase speed if the frequency is high enough. Sound velocimeters, which operate in the megahertz range, provide values of c_o, even in bubbly water because $f >> f_R$ for the significant fractions U(a).

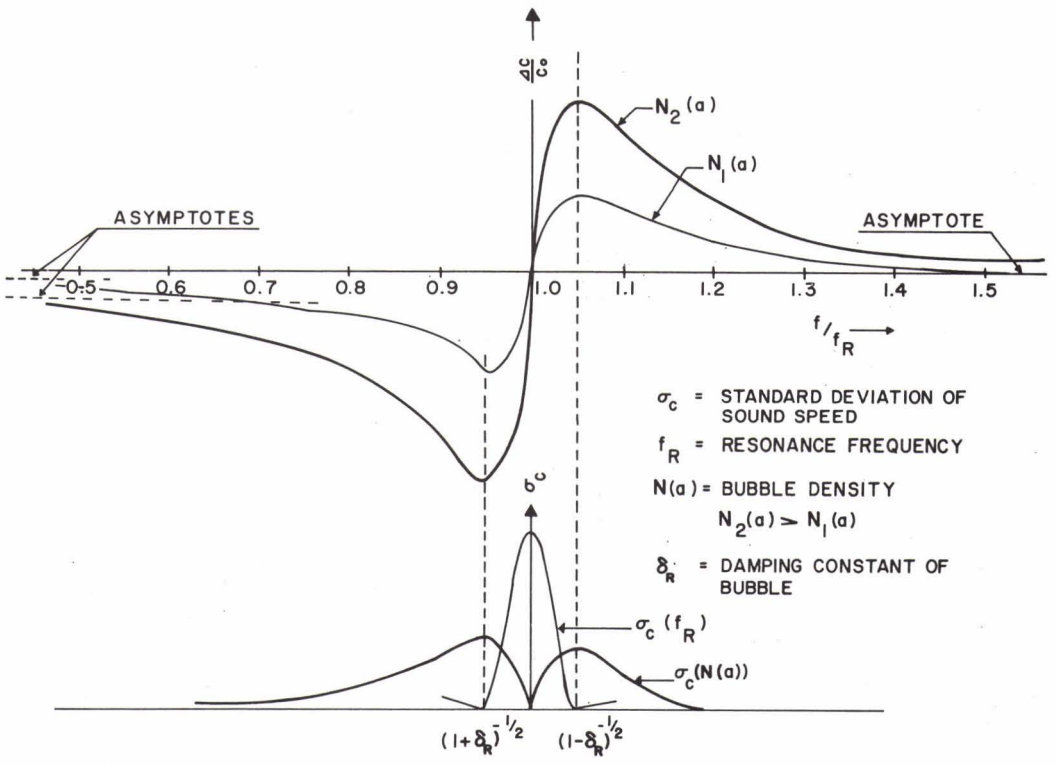

FIG. 1.7
UPPER GRAPH: FRACTIONAL CHANGE OF SPEED OF SOUND FOR A BUBBLY MEDIUM OF ONE BUBBLE RADIUS, a. LOWER GRAPH: STANDARD DEVIATION OF FLUCTUATIONS IN SPEED OF SOUND DUE TO CHANGE OF NUMBER OF BUBBLES PER UNIT VOLUME, $\sigma_c[\ N(a)\ ]$, AND DUE TO CHANGE OF RESONANCE FREQUENCY WITH A CONSTANT NUMBER OF BUBBLES, $\sigma_c(f_R)$

Fig 1.7 shows the dispersion for a bubble resonance frequency, 65 kHz, at which $\delta_R \simeq 0.1$. The abscissa is $z^{-1} = f/f_R$. The ordinate is the fractional change in speed, in units of the fractional change at low frequencies. The maximum and minimum occur at frequencies given approximately by $f = f_R\,(1 \pm \delta_R/2)$. The speeds at these points differ from that in bubble-free water by approximately

$$\pm \frac{1}{2\delta_R}\left(\frac{3U}{2a^2k_R^{\,2}}\right).$$

b) Bubbles of Many Sizes:

The generalization to a bubbly medium of random radii is accomplished by replacing N(a) by n(a) da and U(a) by u(a)da. Because all contributions to the compressibility are very small quantities, they add linearly and the speed of sound in the bubbly region can be written

$$\mathrm{Re}\{\underset{\sim}{c}\} = c_o\left[1 - \frac{3}{2}\int_{a_i}\frac{u(a_i)z_i^{\,2}(z_i^{\,2}-1)\,da_i}{a_i^{\,2}k_{iR}^{\,2}[(z_i^{\,2}-1)^2+\delta_{iR}^{\,2}]}\right] \qquad (1.2.15)$$

The effect of a mixture of bubble sizes is to smear the dispersion curve so that although the magnitudes of the deviation from the bubble-free value are increased, the frequency range between the peak and the trough is also increased.

2. Ocean Experiments

Good agreement between theory and experiment for clean laboratory bubbles has encouraged acoustical exploration for bubbles at sea.

In-situ bubble research has been done with equipment sketched in Fig 2.1a (Medwin 1970) and 2.1b (Medwin et al 1975)

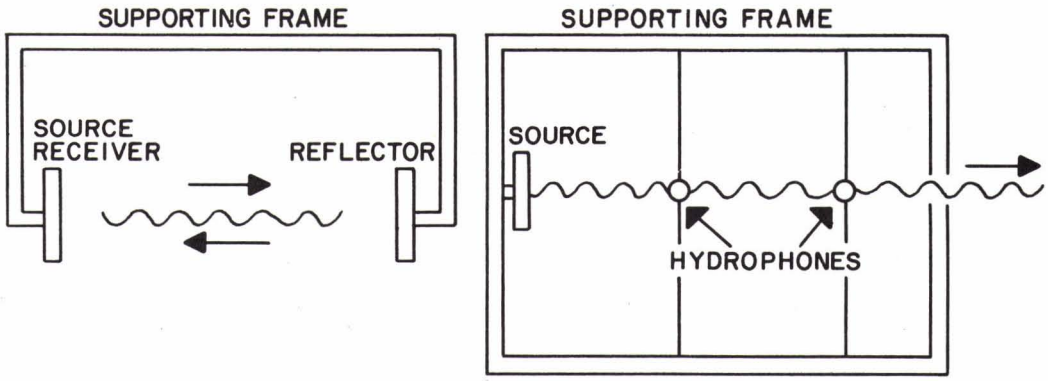

FIG. 2.1
TWO EXPERIMENTAL SCHEMES FOR MEASURING BUBBLE EFFECTS AT SEA:
LEFT: PULSE-ECHO TECHNIQUE; RIGHT: c.w. TECHNIQUE

The devices are generally 2 to 7 meters in extent, and are constructed so that the water medium freely enters the ensonified space.

2.1 Pulse-echo technique

In the pulse-echo technique a sinusoidal wave train of duration approximately 0.5 msec has been used with the transducer electronically switched to receive the reflected echoes. The oscilloscope screen was photographed to record the echo patterns (Fig 2.2).

In principle a single oscillogram may be analyzed in three different ways to obtain the variables of the medium: (1) comparison of the exponential attenuation shown by the echo pattern at sea with that in clean water provides the excess absorption and scattering by objects (assumed to be bubbles) at sea; (2) the relative reverberation between echoes,

compared to the preceding and following echo levels, measures the scatter due to bubbles along the path; (3) the time between echoes permits a calculation of the local speed of propagation. In practice, because of phase shift at the reflectors, the sound speed dispersion due to bubbles at sea has been too small to measure accurately with our pulse-echo system. However, we have determined the extinction cross sections and the scattering cross sections, as a function of frequency at sea. By using both the extinction and the scatter data the absorption cross section can be found and the number of bubbles in a given radius increment per unit volume of water is directly calculable. We assume that the scattering and absorption cross sections of dirty gas bubbles are approximately the same as for clean bubbles.

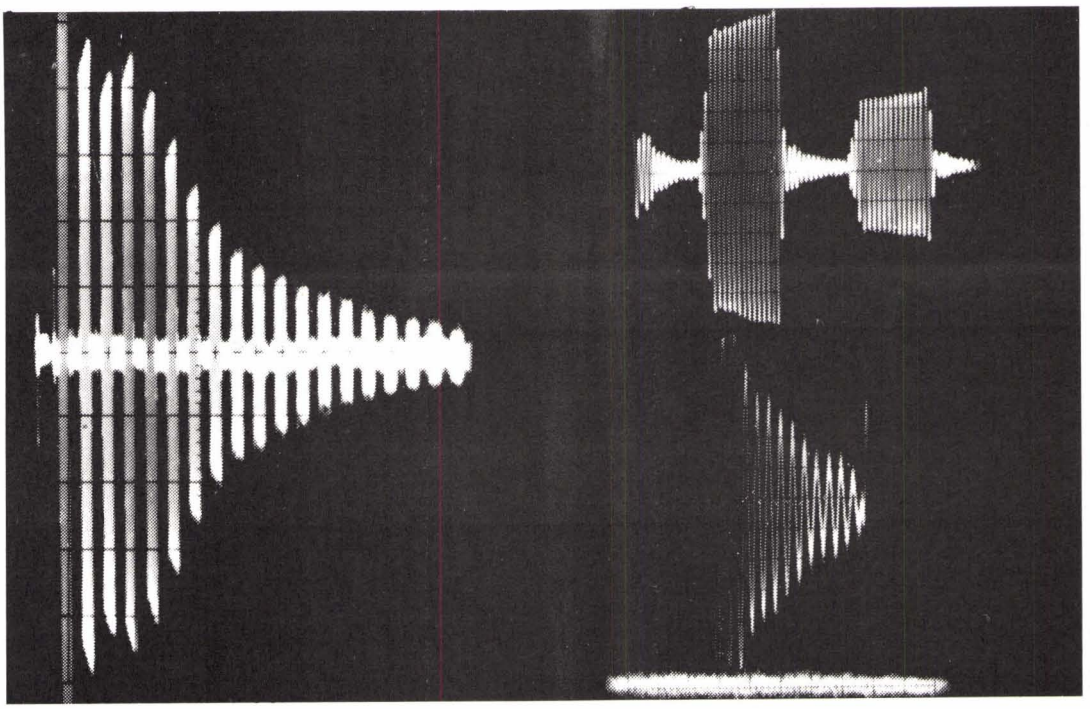

FIG. 2.2
LEFT: OSCILLOGRAM SHOWING 19 ECHOES OF A PULSE-ECHO PATTERN AT 200 kHz. RIGHT: TOP, TWO ECHOES AND BACKSCATTER BETWEEN THEM AT 30 kHz; MIDDLE, AMPLIFIED BACKSCATTER BETWEEN TWO ECHOES; BOTTOM, SYSTEM NOISE LEVEL ON SAME SCALE AS BACKSCATTER

2.2 Continuous wave technique

It is also possible to obtain in-situ bubble information by continuous wave acoustic measurements. (Medwin et al 1975). The study requires only the sound source and two point hydrophones separated by a fixed distance (Fig 2.1) .

The speed is easily found as a function of frequency by measuring the number of wavelengths between the two hydrophones. Then,

$$c = f\lambda = f \frac{x}{M + \phi/360} \qquad (2.1.1)$$

where x is the distance between the two hydrophones, M + Ø/360 is the integral plus fractional number of wave lengths. The number, M, is obtained by using a rough value of the bubble-free speed, c_o, or from a sound velocimeter. A good phasemeter can give Ø to the nearest tenth of a degree. f is known to 1 part in 10^6 by using a frequency synthesizer or stable oscillator and frequency counter. In fact it is the measurement of distance, x, that is the crudest part of the experiment and that limits the absolute accuracy if the high frequency calibration is not used.

The same cw equipment may be used to measure the attenuation between the two hydrophones and, thereby, to assess the bubble density or volume fraction in particular bands of bubble radii. The attenuation can be found by either analogue or digital measurements. Recently we have been analyzing the simultaneous digital time series from the two hydrophones by FFT. This provides both magnitude and phase of the signal at each of the two hydrophones. The ratio of the magnitudes then gives the attenuation. The difference of the phases, used in eq 2.1.1, yields the speed. When a harmonic-rich signal is used for the sound source, both the attenuation and phase shift can be determined, from the same data for a large number of frequencies (Huffman and Zveare 1974). The mini-computer that we use can do the A/D conversion for the two series at rates up to 320 kHz for each channel simultaneously. Therefore, by using 5 kHz sawtooth input we are able to get speeds and attenuations for the 32 harmonics up to 160 kHz.

3. Acoustically Inferred Bubble Populations at Sea

3.1 Assumptions in an acoustical determination

Our conversion from attenuation or dispersion measurements to bubble populations assumes the constants of the physicist's clean, free, air bubble. But bubbles at sea are of other gases, as well as air, and they may have organic skins or other detritus on their surfaces, or, indeed, be parts of phyto-plankton or zoo-plankton. The inferred radius will be affected by these changed conditions, but in no major way. For example, realistic ocean bubble gases include oxygen, carbon dioxide, carbon monoxide, hydrogen sulfide and methane for which the value γ ranges from 1.30 to 1.40. The error in the resonance radius assuming air, instead of the true gas, would be at most 5% according to eq (1.18).

On the other hand, changing bubble gas from air to methane or carbon dioxide, for example, results in a significant increase in σ_e and σ_s because of the different damping constants. At 50 kHz, a sea level bubble at resonance has $\sigma_e = 0.40$ cm^2 if it is of air, whereas it is 0.46 cm^2 for CH_4 and 0.60 cm^2 for CO_2. For the same conditions, σ_s is 0.056 cm^2 for the air bubble, 0.074 cm^2 for CH_4 and 0.13 cm^2 for CO_2. Not knowing the bubble gas thereby degrades the accuracy of the acoustical determination of bubble populations by extinction or backscatter experiments alone.

Since $\sigma_e = \sigma_a + \sigma_s$, and since σ_s increases with bubble radius (see $a > a_R$ in Figs 1.5, 1.6) in spite of the high Q character of the cross sections at resonance the variation of bubble number with bubble radius could conceivably affect its very determination. Fortunately, absorption measurements in tap water (Gavrilov, 1969) and our own work at sea show that the variation of $n(a)da$ with radius lies between a^{-4} and a^{-2}. Under these conditions the integration of eq (1.2.2) converges and the resonance peak, alone, can be used to calculate the bubble density at that resonance radius. It is for this reason that excess attenuation or backscatter data obtained as a function of frequency can be interpreted as bubble radius spectrometry.

Measurements in the near-surface ocean, where bubbles are common, do not produce constant values. This is partly because of the inhomogeneity of the medium and partly because of the orbital motion associated with surface waves. Our selection of a one meter path between the two hydrophones fixes our averaging space for the inhomogeneous ocean. In our

analog work we use an averaging time of 10 to 20 minutes for each frequency. In our digital work, a run takes only 3.2 ms and the temporal variations as well as the averages are identified by repeated measurements.

3.2 Bubble fractions and bubble densities.

Our first ocean bubble experiments were done at the NUC Oceanographic Tower, off San Diego, about 10 years ago. (Medwin 1970). Since that time we have made measurements in BASS Strait, Australia (Medwin et al 1975) and most recently in Monterey Bay (Huffman and Zveare 1974). Nevertheless we feel as innocent in this vastly complicated study as the propagation people must have felt when the first bathythermograph was obtained in the 1930's. What we can say is this: Bubble densities decrease with greater depth; they increase with greater wind speeds; small bubbles are apparently greater in number in the day time than at night, however, for bubbles larger than about 60μ the opposite is true. But this is about all that we have the courage to say at this time.

Figs 3.1 - 3.4 are samples of what we find. This particular case from the MS Thesis of Huffman and Zveare (1974) was observed 0.9 nautical miles from shore, using the research vessel ACANIA at anchor in water of depth 38M on 12-13 November 1974. The wind speed was 2 knots, cloud cover was 25 to 80%, and the ship was surrounded by "thousands" of squid. The data represent averages of 5 runs taken over 15 minutes. At 1630 on 12 November strong attenuations were observed at 15 kHz and 40 kHz. These attenuations are greater, nearer the surface (Fig 3.1) and the predominant bubble populations that they represent are confirmed by the characteristic dispersion shapes at these same frequencies in Fig 3.2. The inferred bubble populations plotted in Fig 3.3 present the typical a^{-4} slope for $f < 60\mu$ and a^{-2} for $f > 60\mu$, that we have consistently seen. Fig 3.4 shows the dependence on time of day; the larger bubbles were somewhat more common at night (sunset was at 1700, sunrise at 0645).

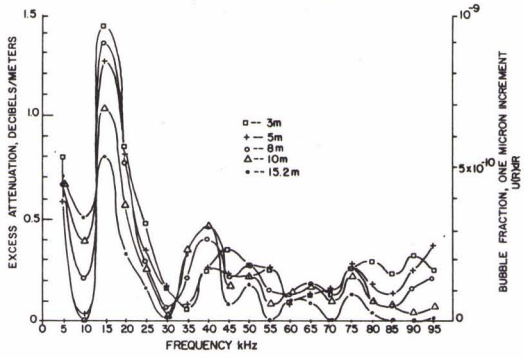

FIG. 3.1
EXCESS ATTENUATION DUE TO BUBBLES AT FIVE DEPTHS, 12 NOV 1974
HUFFMAN AND ZVEARE, 1975

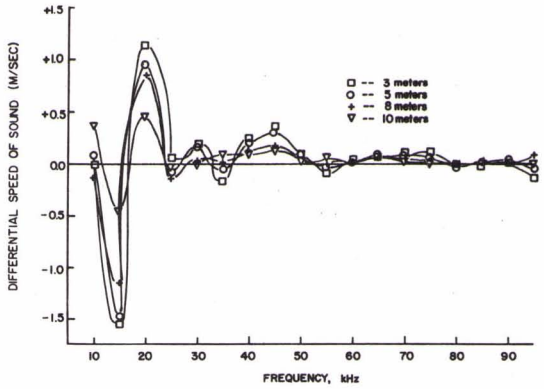

FIG. 3.2
SOUND SPEED DISPERSION AT FOUR DEPTHS, 12 NOV 1974
HUFFMAN AND ZVEARE, 1975

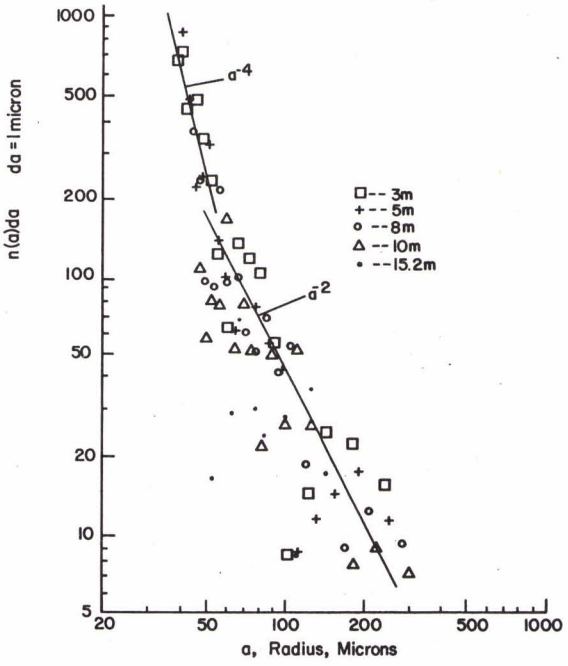

FIG. 3.3
NUMBER OF BUBBLES PER CUBIC METER IN A ONE MICRON RADIUS INCREMENT FROM DATA OF FIG. 3.1
HUFFMAN AND ZVEARE, 1975

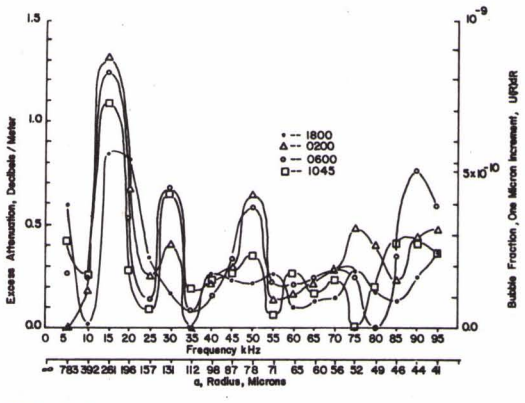

FIG. 3.4
EXCESS ATTENUATION AT 5 m DEPTH AT DIFFERENT TIMES OF DAY. 12, 13 NOV 1974
HUFFMAN AND ZVEARE, 1975

4. Fluctuations due to Bubbles

Sound-speed measurements as a function of frequency, not only reveal bubble presence but they also show that the principal cause of sound-phase fluctuations near the sea surface can be bubble presence rather than temperature microstructure.

Three major sources of speed fluctuations due to bubbles have been identified (Medwin 1974):

(1) Change of speed can be caused by change of total volume fraction of bubbles. From Eq 1.2.13 note that at frequencies well below resonance, change of total volume fraction U causes the variance

$$\mathrm{Var}\{c(U)\} = \left(\frac{3c_o}{2a^2 k_R^2} \right)^2 \mathrm{Var}\{U\}, \quad f \ll f_R \qquad (4.1.1)$$

(2) For a single or predominant bubble radius, it has been determined (Wang and Medwin 1974) that change of number of bubbles will cause peak variances at the frequencies of the speed maximum and minimum given by

$$Z = (1 \pm \delta_R/2).$$

The effect causes peak variances

$$\mathrm{Var}\{c[u(a)]\} = \left[\frac{3c_o(1 \pm \delta_R)}{4a^2 k_R^2 \delta_R} \right]^2 \mathrm{Var}\{u(a)\}. \qquad (4.1.2)$$

The (+) sign, giving the larger variance, occurs at the frequency below resonance. See Fig 1.7.

(3) For a single, or predominant, bubble radius in a distribution, a change of ambient pressure will change the resonance frequency and thereby cause a variation in speed. This effect is also shown in Fig 1.7, where it is identified as producing an rms change $\sigma_c(f_R)$. The magnitude of the effect has been derived and is

$$\mathrm{Var}\{c(Z)\} = \left\{ \frac{Bu(a)\,da\,c_o}{(k_R a)^2 [1 + (D/10)\delta_R^2]} \right\}^2 \mathrm{Var}\{h\} \exp(-2\kappa_0 D),$$

Where $B = 0.083M^{-1}$, Var{c(Z)} is the variance of fluctuations in sound speed due to perturbations of bubble resonance frequency, Var{h} is the variance of height of surface waves in square meters and D is the experiment depth in meters, and K_o is the surface wave number.

An experimental way to distinguish between the three bubble sources of sound-speed variation is by correlation or spectral analysis. (H. Medwin et. al (1975)). For example, in the BASS Strait experiment, at a frequency 24.4 kHz, which is low enough to be essentially unaffected by any specific bubble resonance, the autospectrum of the phase variations is close to Gaussian because of its wide-band random nature (Fig 4.1). But near a predominant bubble resonance frequency, models (2) and (3) are appropriate. Since the frequencies for the two effects are very close it is the magnitude of the cross-correlation with wave height that is the clue to model (3). A particularly large cross correlation was found at frequency 95.6 kHz. Three typical spectra of the fluctuations of sound phase are shown in Figure 4.1. In comparison with 95.6 kHz, all of the spectra for sound frequency 24.4 kHz are flatter and closer to a Gaussian form. They also have near-Gaussian correlation functions and large values of σ_U/U.

On the other hand, the predominant feature of the phase fluctuations for 95.6 kHz is the strong peak at the ocean surface wave peak frequency of 0.17 Hz. All spectra for 95.6 kHz showed this peak which decreased in magnitude with increasing depth. In Figure 4.2 some of the data have been plotted on log-log scale in order to show the power law dependence on frequency. The phase fluctuation spectrum is almost a twin to the ocean surface wave spectrum as it follows the F^{-5} law that would be expected [Phillips, 1966] for a fully-developed sea. The modulation spectral density at 0.3 Hz has been selected to plot against depth (not shown). The slope, which turns out to be approximately exp(-D/4.7 m), is an alternative way to determine the depth dependence of predominant bubble populations.

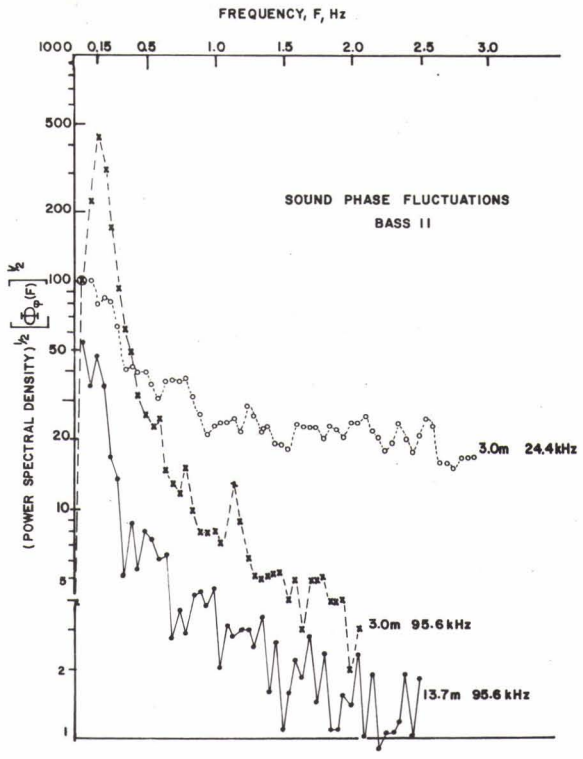

FIG. 4.1
FREQUENCY SPECTRA OF SOUND PHASE FLUCTUATIONS AT 24.4 AND 95.6 kHz DURING BASS EXPERIMENT

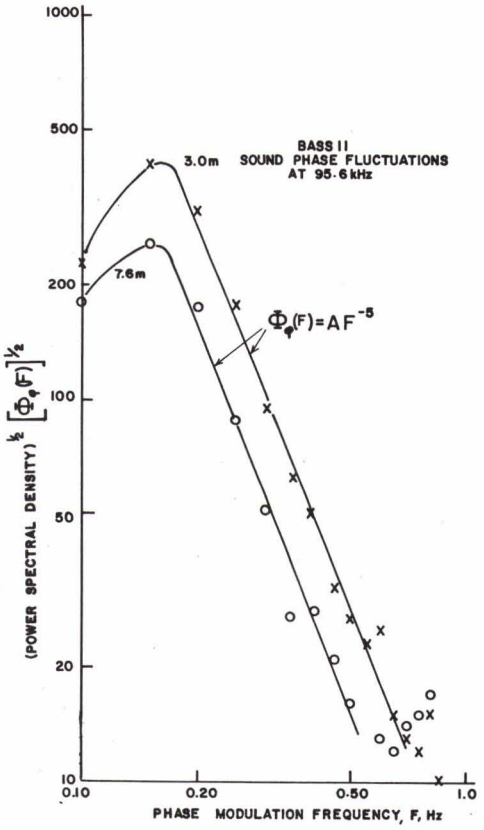

FIG. 4.2
FREQUENCY SPECTRA OF SOUND PHASE FLUCTUATIONS FOR 95.6 kHz SOUND AT DEPTHS 3.0 AND 7.6 m

Acknowledgement

This research was supported by the Office of Naval Research (Code 486.) Mrs. Carol Hickey did the computer calculations of cross sections and damping constants.

REFERENCES

Devin, C., Jr., Survey of thermal, radiation and viscous damping of pulsating air bubbles in water, J. Acoust. Soc. Amer., 31, 1654-1667, (1959).

Eller, A.I., Damping constants of pulsating bubbles. J. Acoust. Soc. Am. 47, 1469-1470,(1970).

Gavrilov, Sov. Phys-Acoust. 15, 22, (1969).

Huffman, T.B. and D.L. Zveare, Sound speed dispersion and inferred microbubbles in the upper ocean. M.S. Thesis, Naval Postgraduate School, Monterey, Ca 93940,(1974).

Medwin et al, Acoustic miniprobing for ocean microstructure and bubbles J. Geophys. Res 80 405-413. (1975).

Medwin, H., In-situ acoustic measurements of bubble populations in coastal ocean waters, J. Geophys. Res., 75, 599-611,(1970).

Medwin, H., Acoustic fluctuations due to microbubbles in the near surface ocean, J. Acoust. Soc. Amer., 56, 1100-1104,(1974).

Phillips, O.M., The Dynamics of the Upper Ocean, p 113, Cambridge University Press, London ,(1966).

Wang, P. C. C., and H. Medwin, Statistical considerations to experiments on the scattering of sound by bubbles in the upper ocean, Quart. J. Appl. Math., 32, 411-425, (1975).

DISCUSSION

DISCUSSION ON SESSION 2

Reported by R.F.J. Winterburn

The absence of MEDWIN to present his paper was regretted by WILLIAMS, who then proposed that the discussion continue on the oceanographic aspects of this session.

LEUTLOFF enquired if the relationship of the size of the swim bladder to the length of the fish was true for only certain species of fish. FOSTER replied that from his review, this relationship seemed to be true for all species, although for each species the values of the parameters are different. There then followed a lengthy discussion as to the validity of this relationship; SCHNEIDER proposed that it could be more meaningful to relate the volume of the fish to the swim-bladder size, as the total length of a fish bears little or no relationship to its actual size. The difficulties of taking this measurement were enunciated by WILLE, whose views were substantiated by GRIMLEY by pointing out that there existed, to his knowledge, a large quantity of literature on this problem, particularly by the Soviets and also a recent paper by Mcartney, NIO Godalming.

DAINTITH suggested that more effort should be put into investigating the acoustic effects of gas bubbles, for which discussion the absence of MEDWIN was greatly felt. WILLIAMS agreed with this suggestion, pointing out that it had been shown that the presence of bubbles, particularly near the surface, could modify the sound field by up to 25 m/s.

Several questions were raised concerning the variability in space and size of bubbles. BACHMANN asked if there was any variation between deep and shallow-water areas; i.e. if the effect of a bottom affected the development or decay of the bubble population. WILLIAMS felt that the photosynthetic development was only true for shallow-water areas, but that much more data was required to validate this. He was then asked if he could give a range of validity to his results, to which he replied that this was difficult in view of the small amount of data. However, he showed a "residue" plot of the data after subtracting his model, pointing out that most of the data agreed within a factor of two. He continued by saying that the wind speed was the most important parameter and needs the most attention.

WILLE asked if it was thought possible for vibration of the bubbles by natural currents to be an additional source of sea noise. WILLIAMS thought that this was highly unlikely, as the natural frequency was very high and the turbulent frequency very low.

INITIAL DISTRIBUTION

	Copies
MINISTRIES OF DEFENCE	
MOD Belgium	1
DND Canada	10
CHOD Denmark	8
MOD France	8
MOD Germany	15
MOD Greece	11
MOD Italy	10
MOD Netherlands	12
CHOD Norway	10
MOD Portugal	5
MOD Turkey	5
MOD U.K.	16
SECDEF U.S.	60
NATO AUTHORITIES	
Defence Planning Committee	3
NAMILCOM	2
SACLANT	10
SACLANTREPEUR	1
CINCWESTLANT/COMOCEANLANT	1
COMIBERLANT	1
CINCEASTLANT	1
COMSUBACLANT	1
COMCANLANT	1
COMMAIREASTLANT	1
COMNORLANT	1
SACEUR	2
CINCNORTH	1
CINCSOUTH	1
COMNAVSOUTH	1
COMSTRIKFORSOUTH	1
COMEDCENT	1
COMSUBMED	1
COMMARAIRMED	1
CINCHAN	1

	Copies
SCNR FOR SACLANTCEN	
SCNR Belgium	1
SCNR Canada	1
SCNR Denmark	1
SCNR Germany	1
SCNR Greece	1
SCNR Italy	1
SCNR Netherlands	1
SCNR Norway	1
SCNR Portugal	1
SCNR Turkey	1
SCNR U.K.	1
SCNR U.S.	2
NATIONAL LIAISON OFFICERS	
NLO Denmark	1
NLO Italy	1
NLO U.K.	1
NLO U.S.	1
NLR TO SACLANT	
NLR Belgium	1
NLR Canada	1
NLR Germany	1
NLR Greece	1
NLR Italy	1
NLR Norway	1
NLR Portugal	1
NLR Turkey	1
ESRO/ELDO Doc. Service	1
ATTENDEES	110